https://doi.org/10.5194/egusphere-2026-3350
Preprint. Discussion started: 31 August 2026

Impact of Low-altitude Meteorological Drone Data Assimilation on Convective-Scale Short-Term Rainfall Forecasts: An Observing System Simulation Study

Juan Zhao[1], Jianping Guo[2,3*], Jidong Gao[4,5], and Honglong Yang[3]

[1]China Meteorological Administration Training Centre, Beijing, China

[2]State Key Laboratory of Severe Weather Meteorological Science and Technology & Specialized Meteorological Support Technology Research Center, Chinese Academy of Meteorological Sciences, Beijing, China

[3]CMA Field Scientific Experiment Base for Low-Altitude Economy Meteorological Support of Unmanned Aviation in Guangdong-Hong Kong-Macao Greater Bay Area, Shenzhen, China

[4]NOAA/National Severe Storm Laboratory, Norman, OK, United States

[5]School of Meteorology, University of Oklahoma, Norman, OK, United States

[*]*Correspondence to*: Dr./Prof. Jianping Guo (Email: jpguocams@gmail.com)

https://doi.org/10.5194/egusphere-2026-3350
Preprint. Discussion started: 31 August 2026

Abstract

This work leverages observing system simulation experiments (OSSEs) to quantify the utility of low-altitude meteorological drone (MD) measurements for convective-scale analyses and short-term rainfall forecasts over the Beijing-Tianjin-Hebei region. Synthetic MD observations of temperature, specific humidity, and horizontal wind are generated from a free-running truth simulation and assimilated into the Weather Research and Forecasting (WRF) model using the National Severe Storms Laboratory three-dimensional variational data assimilation (DA) system. Five sets of sensitivity experiments are conducted to evaluate the impacts of horizontal resolution, observation height, spatial distribution, joint assimilation of thermodynamic and wind observations, and observation errors of MD data, respectively. The results show that assimilation of MD temperature and humidity observations improves both thermodynamic analyses and precipitation forecasts, with the magnitude of benefit strongly dependent on MD network design. Denser MD networks more effectively reduce thermodynamic analysis and forecast errors, leading to better rainband placement, rainfall intensity, and higher quantitative precipitation skill. Among the tested configurations, the 5- and 10-km networks provide the most robust and consistent forecast benefits. Multi-level MD data yield the most balanced improvement, while observations extending to higher levels within the planetary boundary layer are generally more beneficial than those confined to the lowest level alone. Restricting observations to the plain area degrades forecast performance, highlighting the importance of upstream mountainous observations where convection is initiated. In addition, joint assimilation of thermodynamic and wind observations further improves quantitative precipitation forecasts by substantially reducing lower-tropospheric wind errors. Short-term forecast skill is also sensitive to the observation error standard deviations, with inflated wind observation error producing a larger degradation than inflated thermodynamic errors. Overall, it is demonstrated that MD observations have considerable potential to improve convective-scale numerical weather prediction, particularly when the observing network is sufficiently

https://doi.org/10.5194/egusphere-2026-3350
Preprint. Discussion started: 31 August 2026

dense, vertically resolved, and capable of constraining both thermodynamic and dynamical structures within the planetary boundary layer.

https://doi.org/10.5194/egusphere-2026-3350
Preprint. Discussion started: 31 August 2026

1 Introduction

Meteorological uncrewed aircraft systems (UASs), referred to here as meteorological drones (MDs), have emerged as a promising observing platform for reducing persistent observational gaps in the lower atmosphere, especially within the planetary boundary layer (PBL) (Bell et al., 2020; Chilson et al., 2019; Pinto et al., 2021; Reuder et al., 2012). Compared with conventional surface stations and radiosondes, MDs can provide flexible, high-frequency, and vertically resolved in situ observations of key thermodynamic and kinematic variables, including temperature, humidity, and wind. For example, MD systems such as weather-observing UAS (WxUAS) and Small Unmanned Meteorological Observer (SUMO) are capable of providing atmospheric profiles up to approximately 1-2 km above ground level, with vertical resolutions on the order of tens of meters and temporal sampling intervals of several minutes (Chilson et al., 2019; Reuder et al., 2012; Sun et al., 2020). Such capabilities are particularly valuable for convective-scale numerical weather prediction (NWP), as the initiation and early evolution of convection are highly sensitive to the distribution of temperature, moisture, and low-level airflow within the PBL (Chilson et al., 2019; Crook, 1996; Weckwerth and Parsons, 2006).

In recent years, the World Meteorological Organization organized the Uncrewed Aircraft Systems Demonstration Campaign, which investigated the applicability of using MDs as a sustainable and low-cost alternative approach for collecting vertical profiles of meteorological information (Inoue et al., 2025). In the United States, with the rapid development of drone technology and continuing reduction in platform cost, an increasing number of studies have demonstrated substantial progress in the development and application of MD observations (Chilson et al., 2019; De Boer et al., 2024; Jensen et al., 2021; Pinto et al., 2021; Reuder et al., 2012; Segales et al., 2020). Early work established the feasibility of using both fixed-wing and rotary-wing MD (e.g., CopterSonde, Meteodrone) to obtain lower-atmospheric profiles under a range of environments, including complex terrain and polar regions (Reuder et al., 2012). Subsequent efforts further advanced the observational capability of MDs through

https://doi.org/10.5194/egusphere-2026-3350
Preprint. Discussion started: 31 August 2026

improved platform design, sensor integration, and boundary layer profiling applications (Bell et al., 2020; Segales et al., 2020). More recent studies have extended these efforts toward increasingly automated and operational concepts, such as coordinated profiling networks and dense lower-atmospheric observing systems (Chilson et al., 2019; Jensen et al., 2021; Pinto et al., 2021). Meanwhile, MD observations have been explored through data assimilation (DA) experiments for a variety of applications, including fog prediction, convective storms, coastal rainfall, and polar boundary layer forecasts, with generally positive impacts on lower-tropospheric analyses and short-term forecasts (Jensen et al., 2021; Leuenberger et al., 2020; Pinto et al., 2024).

In China, typhoon-oriented meteorological drone observations have expanded markedly in recent years, from the first upper-air integrated unmanned aerial vehicle (i.e. HAIYAN-I) typhoon sounding experiment in 2020 to coordinated maneuvering observations over the South China Sea in 2023 and multi-aircraft typhoon campaigns in 2024 (Wen et al., 2025). This reflects a growing capability for targeted offshore profiling and dropsonde observations in tropical cyclones. Since late 2024, low-altitude meteorological development agenda for China Meteorological Administration has placed increasing emphasis on the deployment of low-altitude observing systems, with particular focus on meteorological drones. Under this framework, MDs are expected to support fixed-point profiling, route-based observations, and targeted mobile observations, primarily within the low-altitude atmosphere below 1000 m, with extensions up to 3000 m when needed. These observations are intended to support a range of typical low-altitude economy applications, including cargo logistics, passenger transport, emergency rescue and disaster response, cultural and tourism activities, agricultural and forestry protection, ecological conservation, and so on. In recent years, several pilot programs in China have begun exploring low-altitude meteorological observation systems based on MD platforms, including low-altitude meteorological observation testbeds in Shenzhen, boundary-layer profiling experiments in Shanxi, and route-based MD observation

https://doi.org/10.5194/egusphere-2026-3350
Preprint. Discussion started: 31 August 2026

campaigns in Nanjing aimed at supporting low-altitude flight operations. Although these developments indicate growing international interest in MD applications, there is little peer-reviewed published research investigating the potential benefit of low-altitude MD observations within this emerging low-altitude meteorological framework, particularly from the perspective of observing network design.

Despite the growing availability of MD observations, their impact on convective-scale NWP remains insufficiently investigated. As routine operational MD observations remain quite limited in world meteorological community, observing system simulation experiments (OSSEs) provide an effective framework for evaluating their potential forecast value before nationwide deployment. In an OSSE, synthetic observations generated from a realistic nature run are assimilated into a forecast system, allowing the impacts of observation type, network configuration, spatial distribution, and sampling strategy to be examined in a controlled manner (Hoffman and Atlas, 2016). In mesoscale and convective-scale NWP, OSSEs have been widely used to assess the potential impact of new observing systems (Hu et al., 2017; Huang et al., 2022; Huo et al., 2023; Zhang and Pu, 2010; Zhao et al., 2021a, 2025). In the context of MD observations, OSSEs are especially useful because they allow key design questions, such as network density, observation height, deployment area, and observation error specification, to be tested before operational implementation (Murdzek et al., 2026).

The main motivation of this study is therefore to explore, through an OSSE framework, the potential value of MD observations for convective-scale analyses and short-term precipitation forecasts over the Beijing-Tianjin-Hebei (BTH) region as an example, and to assess the implications for future MD network design. The BTH region is one of China’s most densely populated and economically developed areas, characterized by complex terrain including the Taihang and Yanshan Mountains to the west and north, which strongly modulate local convective weather through influences on PBL thermodynamic and dynamical structures (Jiang et al., 2021; Li et al., 2024; Zhang et al., 2018). Another motivation for selecting this study region is that

https://doi.org/10.5194/egusphere-2026-3350
Preprint. Discussion started: 31 August 2026

high-impact severe weather events occur frequently, especially in summer. Several related questions will also be addressed. How does the horizontal resolution of MD network impact convective analyses and heavy rainfall forecast in the BTH region? How sensitive is the forecast skill to observation height and deployment area within the PBL? Does the joint assimilation of MD thermodynamic and wind data provide added benefit over the thermodynamic observations alone? To what extent do the analyses and forecasts depend on the assumed MD observation errors? Ultimately, this study seeks to clarify the role of low-altitude MD observations in convective-scale NWP and to provide guidance for the design of future MD observing networks.

Following the Introduction, Section 2 introduces the forecast model and DA system. Section 3 describes the truth and background simulations, synthetic MD observations, and experimental design. Section 4 presents analysis and forecast results from DA sensitivity experiments. Section 5 summarizes key findings and conclusions.

2 Model and DA System

Version 3.7.1 of the Weather Research and Forecasting (WRF) Model with the Advanced Research WRF (ARW) dynamical core (Skamarock et al., 2008) is employed for both DA and forecast experiments. Simulations are performed on a 1-km resolution domain with 630×720 horizontal grid points and 51 vertical levels, extending to a model top at 50 hPa. The model domain is centered over northern China, covering the BTH region (Fig. 3a). The physical parameterization suite includes the National Severe Storms Laboratory (NSSL) two-moment four-ice bulk microphysics scheme (Mansell et al., 2010; Mansell and Ziegler, 2013; Ziegler, 1985), the Rapid Radiative Transfer Model (RRTM) longwave radiation scheme (Mlawer et al., 1997), the Dudhia shortwave radiation scheme (Dudhia, 1989), the Rapid Update Cycle (RUC) land surface model (Benjamin et al., 2004), and the Yonsei University (YSU) planetary boundary layer scheme (Hong et al., 2006).

https://doi.org/10.5194/egusphere-2026-3350
Preprint. Discussion started: 31 August 2026

This study adopts the NSSL Experimental Warn-on-Forecast three-dimensional variational DA system (NSSL3DVAR) (Gao et al., 2013, 2016; Gao and Stensrud, 2014; Wang et al., 2019; Zhuang et al., 2016), which is developed for convective-scale NWP and severe storm forecasting (Gao et al., 2024; Heinselman et al., 2024). Within the NSSL3DVAR framework, the analysis is obtained through minimization of a cost function composed of the background term J_b, the observation term J_o, and the constraint term J_c:

$$J = J_b + J_o + J_c = \frac{1}{2}(\mathbf{x}-\mathbf{x}_\mathrm{b})^\mathrm{T}\mathbf{B}^{-1}(\mathbf{x}-\mathbf{x}_\mathrm{b}) + \frac{1}{2}(H(\mathbf{x})-\mathbf{y}_\mathbf{o})^\mathrm{T}\mathbf{R}^{-1}(H(\mathbf{x})-\mathbf{y}_\mathbf{o}) + J_c, \quad (1)$$

where $\mathbf{x}$ and $\mathbf{x}_\mathrm{b}$ denote the analysis and background state vectors; $\mathbf{y}_\mathrm{o}$ is the observation vector; and H represents the observation operator that maps model variables into observational space. The matrices $\mathbf{B}$ and $\mathbf{R}$ correspond to the background and observation error covariance matrices, respectively. The weak constraint term J_c incorporates the elastic mass continuity equation and a diagnostic pressure equation constraint, which are formulated to improve dynamical consistency for convective-scale DA (Gao et al., 2004; Ge et al., 2012). The control variables in the analysis system include the three-dimensional wind components, pressure, potential temperature, water vapor mixing ratio, and hydrometeor mixing ratios for cloud water, rain, ice, snow, and graupel (Gao and Stensrud, 2012).

The NSSL3DVAR system is capable of efficiently assimilating a wide range of high-resolution observations, including radar radial velocity and reflectivity (Gao et al., 2013, 2016), radar wind profiler (Zhao et al., 2025), conventional sounding and surface measurements (Hu et al., 2019), and several satellite-derived products, such as cloud water path (Pan et al., 2021), total precipitable water (Jones et al., 2018; Pan et al., 2018), Geostationary Lightning Mapper (GLM)-retrieved water vapor (Fierro et al., 2019; Hu et al., 2020), and atmospheric motion vectors (Mallick and Jones, 2020; Zhao et al., 2021b, 2022). To help address the scarcity of observations in the PBL, which plays an important role in forecasting high-impact weather such as thunderstorms and dense fog, a MD assimilation module is developed and incorporated into the DA system. Given the operational demand for rapid updates in

https://doi.org/10.5194/egusphere-2026-3350
Preprint. Discussion started: 31 August 2026

severe weather forecasting, the computational efficiency of the 3DVAR framework makes it well suited for short-cycle applications (e.g., 15-min update intervals; Hu et al., 2021). As the primary objective here is to evaluate the impact of assimilating MD data on convective-scale analyses and short-term forecasts, the ensemble-based background error covariance option available in the DA system is not employed (Gao et al., 2016; Gao and Stensrud, 2014; Wang et al., 2019). Instead, the background error covariance matrix is specified using a static formulation, constructed as the product of a diagonal matrix of background error standard deviations and a spatial recursive filter (Gao et al., 2004, 2013). The standard deviations for control variables are estimated from multi-year statistics of 3-h forecasts from the Rapid Update Cycle (RUC; Benjamin et al., 2004a) system (Fierro et al., 2019; Pan et al., 2021). Spatial correlations are modeled using the recursive filter approach of Purser et al. (2003a, b), which can be applied in multiple passes with distinct correlation length scales to represent the characteristic scales of assimilated observations. Taking the baseline 5-km MD data assimilation experiment (MD_H5) as an example, the horizontal correlation length scales are specified as 10 km in the first pass and 5 km in the second pass, while the corresponding vertical correlation length scales are set to two and one grid points, respectively. The chosen correlation scales are proportional to the observation spacing, reflecting the characteristic scales resolved by the MD network.

3. Experimental design

3.1 Truth run and background run configuration

In the OSSE framework, synthetic MD observations are produced by perturbing the model “truth” with prescribed observation errors. The truth simulation is generated using the WRF model initialized with the fifth-generation European Centre for Medium-Range Weather Forecasts reanalysis dataset (ERA5; Hersbach et al., 2020; Hoffmann et al., 2019), following the model configuration and physical parameterizations described in Sect. 2. A heavy rainfall event that occurred over the BTH region on 29 July 2024 is selected as the test case for constructing the OSSE and

https://doi.org/10.5194/egusphere-2026-3350
Preprint. Discussion started: 31 August 2026

examining the influence of different MD network configurations on short-term convective precipitation forecasts. This event occurred in a favorable synoptic environment characterized by the periphery of the subtropical high, an eastward-propagating upper-level trough, and a low-level jet, which together provided abundant moisture and strong vertical wind shear conductive to organized convection. For the truth run, the WRF model is initialized with ERA5 and integrated forward for 18 h, with lateral boundary conditions updated hourly from the ERA5 data.

This study adopts an OSSE framework based on an identical-twin design, in which the same numerical model is used for both the truth simulation and the forecast system. Consequently, the results should be interpreted with the limitation that such configuration may lead to overly optimistic estimates of observational impacts (Hoffman and Atlas, 2016). To partially alleviate this issue, the first-guess background simulation (NoDA) is initialized and forced with forecasts from the National Centers for Environmental Prediction (NCEP) Global Forecast System (GFS), which differ from those used in the truth simulation.

The 6-h accumulated precipitation forecasts from both the truth and background runs are evaluated against rainfall estimates from the China Meteorological Administration Multisource Precipitation Analysis System (CMPAS), a gauge-radar-satellite merged precipitation product (Pang et al., 2021) with a spatial resolution of $0.01° \times 0.01°$ and an hourly temporal resolution (Fig. 1). The CMPAS estimates (Fig. 1a and b) reveal a well-organized southwest-northeast-oriented precipitation band extending across the BTH region, with several embedded precipitation cores exceeding 50-100 mm. The most intense rainfall is mainly located over Beijing and eastern Hebei Province, indicating a typical organized convective precipitation system. The truth simulation (Fig. 1c and d) reproduces the primary precipitation structure reasonably well, including the orientation and spatial extent of the main rainband, and also captures its overall propagation tendency. The dominant rainfall centers are generally well reproduced, although the simulated field appears somewhat smoother and shows slight spatial displacement relative to the CMPAS

https://doi.org/10.5194/egusphere-2026-3350
Preprint. Discussion started: 31 August 2026

estimates. Despite these differences, the rainfall distribution and intensity are broadly consistent with the CMPAS product, indicating that the truth run provides a physically realistic representation of the convective system for the OSSE framework. In contrast, the NoDA forecasts (Fig. 1 e and f) show larger departures from the CMPAS product. Although a precipitation band is still evident, its position and structure differ more substantially from the observed rainfall pattern, and the localized heavy-rainfall cores are less well captured. These deficiencies indicate considerable errors in the background forecast prior to DA. The discrepancies among the background forecast, the truth simulation, and the multi-source precipitation product provide a meaningful testbed for evaluating the potential benefits of assimilating additional observations. In particular, given that convective precipitation systems are highly sensitive to thermodynamic and kinematic conditions in the PBL, this case offers a suitable scenario for assessing the potential contribution of MD observations to improving convective-scale analyses and short-term precipitation forecasts.

https://doi.org/10.5194/egusphere-2026-3350
Preprint. Discussion started: 31 August 2026

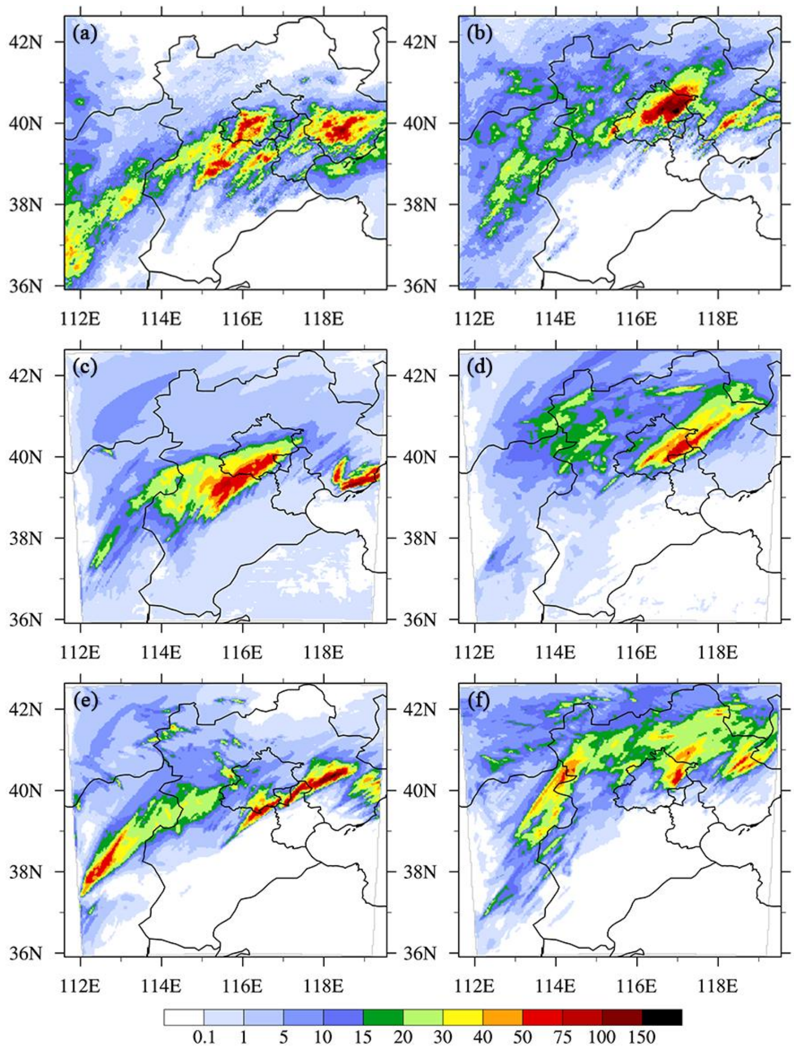

Figure 1. **Comparison of precipitation forecasts from Truth and NoDA experiments with multi-source merged precipitation product.**

The 6-h accumulated precipitation fields (mm, shaded) from 1800 UTC 29 July to 0000 UTC 30 July (left), and from 0000 UTC 30 July to 0600 UTC 30 July, 2024 (right) from (a)–(b) the China Meteorological Administration Multisource Precipitation Analysis System (CMPAS) rainfall estimates, (c)–(d) Truth simulations, and (e)–(f) NoDA experiments.

https://doi.org/10.5194/egusphere-2026-3350
Preprint. Discussion started: 31 August 2026

3.2 Synthetic meteorological drone observations

Meteorological drones have been increasingly developed to address observational gaps in the PBL by providing high-resolution measurements of key thermodynamic and kinematic variables, including temperature, humidity, and wind (Houston et al., 2020; Inoue et al., 2025; Pinto et al., 2021). MD observations are typically conducted within the lowest 1-3 km of the atmosphere, where many weather-sensitive processes relevant to short-term forecasting occur, and commonly involve vertical profiling or targeted flight operations with temporal resolutions of seconds and vertical resolutions on the order of tens of meters (Bell et al., 2020; Houston et al., 2020). Currently, MDs in China employ both multirotor and fixed-wing platforms to provide vertical profiling and targeted mobile data. The observations are also characterized by high temporal and vertical resolutions, with various horizontal resolutions depending on flight mode, ranging from point-based profiling to kilometer-scale transects. Future MD development plans are expected to focus primarily on the low-altitude airspace below 1 km, including targeted observations within representative operating layers such as about 120 m (referred to as Class W airspace), 300 m (referred to as Class G airspace), and 600 m for urban and general aviation applications.

In this study, the synthetic profiles of temperature (T), specific humidity (Q_v), zonal and meridional wind components (U and V) are specified at 120-, 300-, and 600-m altitudes to represent realistic MD deployment in China (Fig. 2). These variables are extracted from the truth thermodynamic and kinematic fields using linear interpolation in the vertical. Simulated MD observations are then synthesized by averaging the truth fields onto coarser grids. Horizontal resolutions of 5, 10, 20, and 40 km are adopted to mimic the spatial representativeness of real MD observations (Fig. 3). It is noted that Fig. 3b displays only a subset of the full model domain (black box in Fig. 3a) to more clearly illustrate the distribution of observational grids at different resolutions. The synthetic observations are generated at 15-min intervals. To account for measurement uncertainty, Gaussian random errors with a mean of zero are

https://doi.org/10.5194/egusphere-2026-3350
Preprint. Discussion started: 31 August 2026

added to the synthetic observations. The standard deviations are set to 1 K for temperature, 1 g kg^{-1} for specific humidity, and 1 m s^{-1} for wind, which are broadly consistent with the range of observational uncertainties reported in previous studies (Bell et al., 2020; Kay et al., 2025; Murdzek et al., 2026; Pinto et al., 2021).

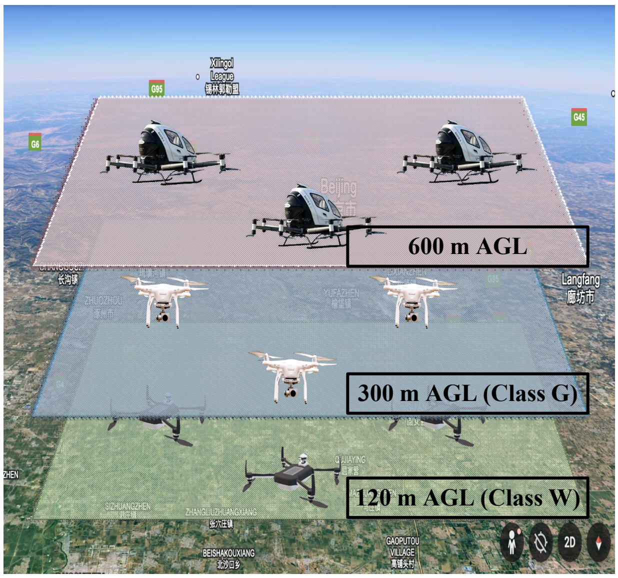

Figure 2. Schematic configuration of multi-layer meteorological drone (MD) observational framework.

Three tiers of MD sampling heights are illustrated: low-level observations at 120 m above ground level (AGL, Class W airspace), mid-level observations at 300 m AGL (Class G airspace), and upper-level observations at 600 m AGL. Base terrain imagery modified from Google Earth.

https://doi.org/10.5194/egusphere-2026-3350
Preprint. Discussion started: 31 August 2026

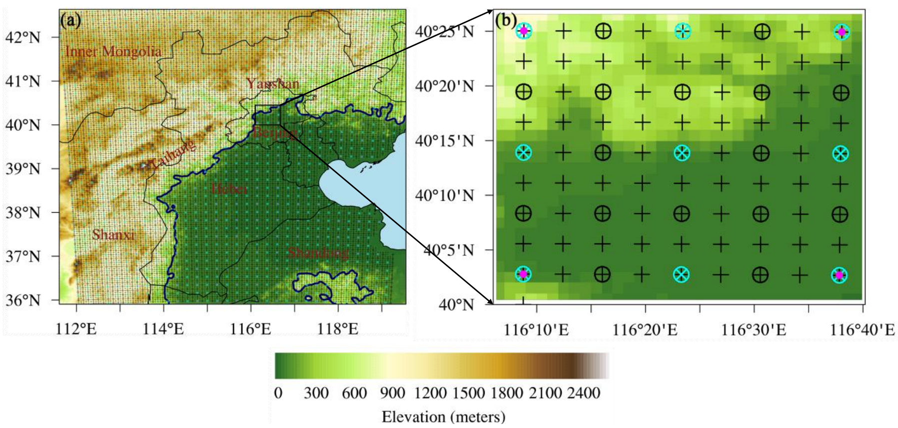

Figure 3. Overview of the numerical simulation domain and spatial layout of MD observation grids with four distinct horizontal resolutions.

(a) Full modeling domain overlaid on shaded terrain elevation; color bar denotes elevation in meters, ocean regions are shaded light blue. The simulated MD networks with horizontal spacings of 5 km (black crosses), 10 km (black circles), 20 km (cyan circles), and 40 km (magenta dots) are also shown. The thick blue contours mark the 300-m elevation boundary separating mountain and plain terrain. Red text labels the major administrative regions (Beijing, Hebei, Shanxi, Shandong, and Inner Mongolia) as well as the Taihang and Yanshan Mountains. The black rectangular box outlines the subdomain magnified in panel (b). (b) Magnified subdomain showing MD sampling points at four horizontal grids.

https://doi.org/10.5194/egusphere-2026-3350
Preprint. Discussion started: 31 August 2026

As our primary objective is to quantify the effects of assimilating thermodynamic and kinematic observations from different MD networks on convective-scale analyses and short-term severe weather forecasts, only synthetic MD data are assimilated in this study. Conventional observations, including radiosondes and surface stations, as well as satellite and radar measurements, are excluded. This experimental design allows a more direct attribution of forecast impacts to the simulated MD observations, although it may also overstate their relative contribution (Hoffman and Atlas, 2016). As a result, the DA experiments are designed to evaluate the upper bound of the information content provided by MD observations, rather than their marginal impact when added to an operational DA system that already assimilates a broad range of conventional and remote-sensing observations.

3.3 DA experiment setup

To emulate an operational rapid-update forecasting environment, the OSSE is configured with a 6-h cycling framework with analyses updated every 15 min, broadly following the real-time Warn-on-Forecast System (WoFS) Spring Forecast Experiment workflow (Heinselman et al., 2024; Hu et al., 2021; Jones et al., 2018). GFS forecasts are used to provide both the initial and lateral boundary conditions for all simulations. To serve as a reference, an experiment without assimilating any observations is carried out and referred to as NoDA. To assess the impact of different MD network configurations on convective-scale NWP, five sets of DA sensitivity experiments are conducted:

1. The first set of experiments examines the impact of MD observations with different horizontal resolutions (5, 10, 20, and 40 km) in order to assess how observation density influences analyses and forecasts. Among these experiments, MD_H5, in which synthetic observations with 5-km grid spacing are assimilated, is selected as the baseline reference for subsequent sensitivity tests.
2. The second set investigates the sensitivity to observation height by separately assimilating MD observations at 120, 300, and 600 m,

https://doi.org/10.5194/egusphere-2026-3350
Preprint. Discussion started: 31 August 2026

respectively, while keeping the horizontal resolution fixed at 5 km. These experiments are designed to examine the relative contribution of observations collected at different altitudes of the PBL.

3. For the third set, assimilated MD observations are distributed only over the plain area, defined here as regions with terrain elevation below 300 m (thick blue contours in Fig. 3a). This design tests whether the forecast impact depends on the spatial deployment of the MD network.
4. The fourth set evaluates the added value of MD wind observations. Whereas only temperature and humidity observations are assimilated in the first three sets, this set of experiment assimilates thermodynamic data together with horizontal wind observations, thereby quantifying the contribution of kinematic information to the analyses and forecasts.
5. The fifth set explores the sensitivity of the analyses and forecasts to prescribed observation errors. Separate experiments are conducted by inflating the observation error assigned to temperature, humidity, and wind, respectively, in order to assess how the assumed uncertainty of each variable affects the analyses and subsequent forecasts.

Basic configurations for each set of sensitivity experiments implemented in the variational system are listed in Table 1. In addition to assessing the impact of synthetic MD observations on convective-scale DA and NWP, sensitivity experiments in each set are compared with the baseline experiment (MD_H5) to isolate the effects of horizontal resolution, observation height, spatial distribution, joint assimilation of thermodynamic and wind observations, and prescribed observation errors, respectively.

https://doi.org/10.5194/egusphere-2026-3350
Preprint. Discussion started: 31 August 2026

Table 1. List of DA sensitivity experiments based on various configurations of the meteorological drone (MD) network over the Beijing-Tianjin-Hebei region.

Experiment		Horizontal resolution (km)	Detection height (m)	Observation variables	Observation error (standard deviations)
Set 1	MD_H40	40	120/300/600	T, Q_v	1 K, 1 g kg^{-1}
	MD_H20	20			
	MD_H10	10			
	MD_H5	5			
Set 2	MD_H5_Z120	5	120	T, Q_v	1 K, 1 g kg^{-1}
	MD_H5_Z300		300		
	MD_H5_Z600		600		
Set 3	MD_H5_Plain	5	120/300/600	T, Q_v	1 K, 1 g kg^{-1}
Set 4	MD_H5_UV	5	120/300/600	T, Q_v, U, V	1 K, 1.0 g kg^{-1}, 1 m s^{-1}
Set 5	MD_H5_ERR_T	5	120/300/600	T, Q_v, U, V	3 K, 1 g kg^{-1}, 1 m s^{-1}
	MD_H5_ERR_Q				1 K, 3 g kg^{-1}, 1 m s^{-1}
	MD_H5_ERR_UV				1 K, 1 g kg^{-1}, 3 m s^{-1}

4 Results and discussion

The impact of assimilating synthetic MD observations on convective-scale NWP is assessed from the perspectives of initial field structure, evolution of analysis and forecast errors, and precipitation forecast skill. First, the influence of MD DA on the model initial conditions is diagnosed through detailed analyses of the spatial structures of temperature, humidity, and wind fields. Additionally, time series and vertical profiles of root-mean-square errors (RMSEs) for thermodynamic and

https://doi.org/10.5194/egusphere-2026-3350
Preprint. Discussion started: 31 August 2026

kinematic variables are computed throughout the DA cycles and subsequent 6-h free forecasts for each experimental configuration. Finally, the influence on short-term precipitation forecast is examined through both qualitative inspection and quantitative verification of accumulated rainfall against the truth simulation. Quantitative precipitation forecast skill is evaluated using a neighborhood-based approach with a 12-km radius across multiple accumulated precipitation thresholds, including the equitable threat score (ETS, Clark et al., 2010) and contingency-table metrics such as probability of detection (POD), false alarm ratio (FAR), success ratio (SR), frequency bias (BIAS), and critical success index (CSI).

4.1 Sensitivity to horizontal resolution

4.1.1 Impact on thermodynamic analyses and forecasts

To illustrate how the assimilation of MD observations with different horizontal resolutions modifies the thermodynamic analyses, Figures 4 and 5 present the 850-hPa temperature and 925-hPa specific humidity fields, respectively, together with the corresponding wind vectors from the truth run and the differences between each experiment and the truth simulation at the end of analysis cycles. Figures 4b–f and 5b–f show the temperature and specific humidity departures of NoDA, MD_H40, MD_H20, MD_H10, and MD_H5 relative to the truth run, respectively; these departures are interpreted here as analysis errors. Positive (negative) values indicate a warm (cold) bias relative to the truth in Fig. 4, whereas in Fig. 5 they indicate a moist (dry) bias. In the truth simulation, a pronounced northwest–southeast temperature gradient is evident over the BTH region, with relatively cool air over the northern and northwestern mountainous areas and warmer conditions over the southeastern plains (Fig. 4a). The NoDA experiment exhibits widespread warm biases over much of western and northern domain, especially near the Yanshan and Taihang Mountains, while weak cold biases are found over northeastern Hebei, northern Shandong, and the adjacent coastal waters (Fig. 4b). This indicates that the background run does not adequately represent the mesoscale thermal structure. Assimilation of MD data clearly reduces these temperature errors, although the magnitude of improvement depends on

https://doi.org/10.5194/egusphere-2026-3350
Preprint. Discussion started: 31 August 2026

the horizontal resolution of MD observation network. The MD_H40 experiment still retains relatively large warm and cold bias patches, particularly in the Taihang Mountains upstream of Beijing (Fig. 4c). Sequential refinement of horizontal sampling grid spacing from 40 to 20, 10, and 5 km produces steady reductions in both the spatial extent and amplitude of the temperature bias (Fig. 4d-f).

Among all experiments, MD_H5 produces the smallest and smoothest temperature departures from the truth run over most of the domain (Fig. 4f), which suggests that the densest MD network most effectively constrains the lower-tropospheric thermal analysis. Nevertheless, some residual errors remain, especially near the northern mountainous region, implying that thermodynamic structures in terrain-influenced areas are still difficult to fully recover even with relatively dense MD observations. For all DA experiments, the wind analysis errors are only marginally reduced, as assimilating thermodynamic observations alone provides only limited adjustment to the flow field.

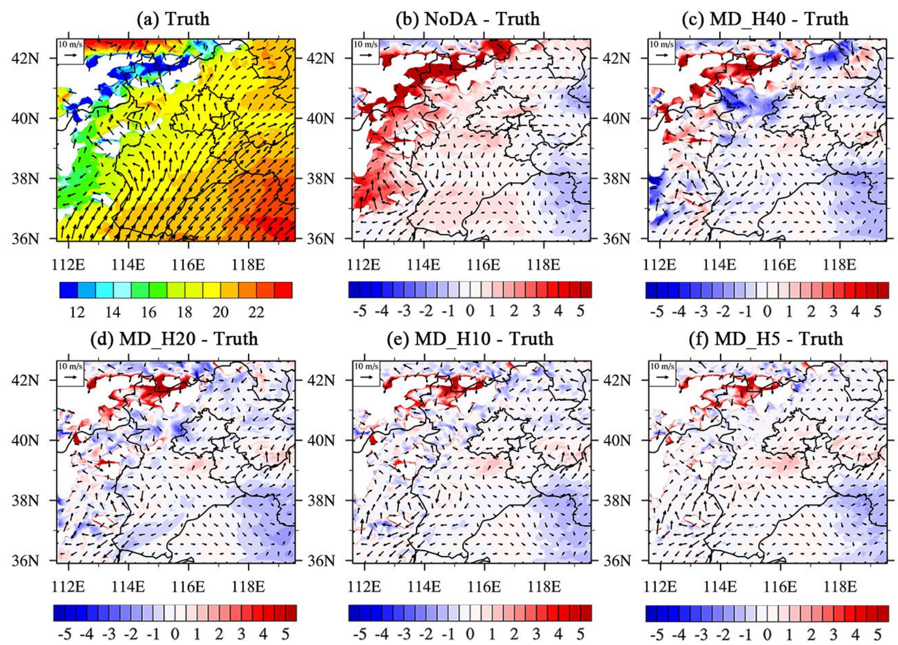

Figure 4. Horizontal resolution sensitivity of 850-hPa temperature analysis bias at 1800 UTC on 29 July 2024, the final time step of the data assimilation cycling. (a) Shaded 850-hPa temperature (°C) and horizontal wind vectors from the truth run.

https://doi.org/10.5194/egusphere-2026-3350
Preprint. Discussion started: 31 August 2026

Panels (b)–(f) show 850-hPa temperature and wind vector bias (experiment minus truth): (b) NoDA, (c) MD_H40, (d) MD_H20, (e) MD_H10, and (f) MD_H5 experiments. Red shading denotes positive temperature bias relative to the truth run, while blue shading denotes negative bias.

Figure 5 further shows that the impact of MD horizontal resolution on the humidity field is broadly consistent with that found for the temperature analysis. In the truth simulation, the low-level jet transports the moist and unstable airmass across the southeastern plains and Bohai coastal area (Fig. 5a). The NoDA experiment produces substantial dry biases over Beijing and central-southern Hebei, together with moist biases along the northern belt near the Yanshan Mountains and along a second southwest-northeast-oriented belt southeast of Beijing (Fig. 5b). Generally, assimilation of MD observations substantially reduces these errors in the background moisture structure, and the improvement becomes more evident as the horizontal resolution of simulated MD observations increases (Fig. 5c-f). In particular, large dry biases over Beijing and central-southern Hebei are progressively weakened, and the two parallel southwest-northeast-oriented moist bias bands are also reduced. Among all experiments, MD_H5 yields the smallest humidity departures from the truth and provides the best overall recovery of the mesoscale moisture pattern (Fig. 5f). Only minor residual humidity errors remain, mainly near the northern mountainous region and over offshore areas where no MD observations are available. This indicates that the moisture field is generally well adjusted after assimilation of MD data, although terrain-influenced regions remain more difficult to constrain than the plains.

https://doi.org/10.5194/egusphere-2026-3350
Preprint. Discussion started: 31 August 2026

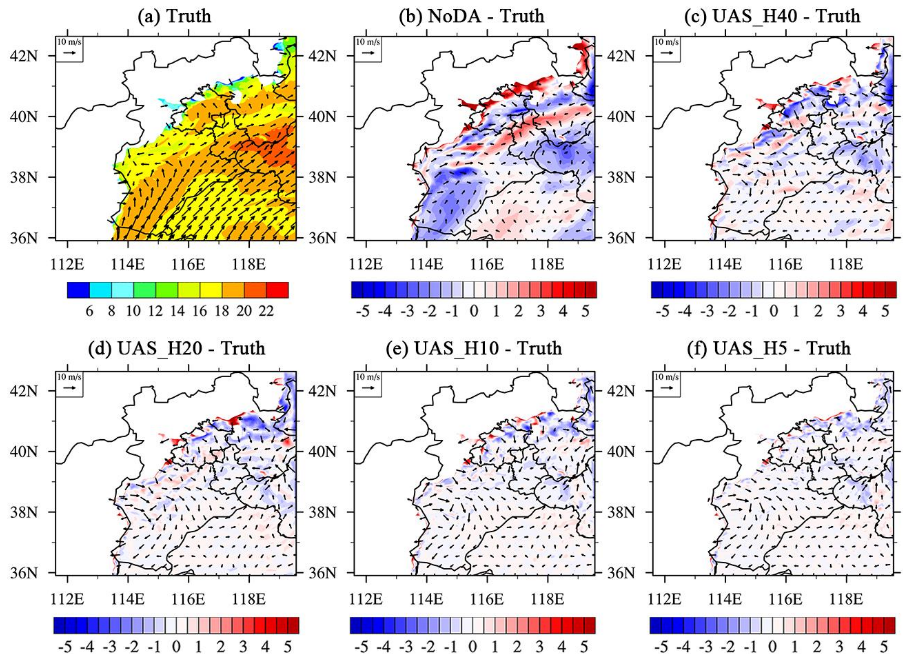

Figure 5. Same as Fig. 4, but the 925-hPa specific humidity (g kg^{-1}) and wind vectors.

The influence of the horizontal resolution of MD observations on the thermodynamic analyses and forecasts can also be directly assessed by examining the RMSEs of temperature and humidity fields during the 6-h assimilation cycles and subsequent 6-h free forecasts. Time series of domain-averaged RMSEs from the MD_H40, MD_H20, MD_H10, and MD_H5 experiments are compared in Fig. 6. During the 6-h cycling period, RMSEs of both temperature and specific humidity increase in all experiments; however, a clear dependence on observation density is evident. Finer MD networks consistently produce smaller errors, with MD_H5 giving the lowest RMSEs, followed by MD_H10, MD_H20, and MD_H40. This ordering agrees well with the diagnostic results shown in Fig. 4 and 5. Moreover, the same ranking is retained in the subsequent 6-h free forecasts, indicating that the improved thermodynamic fields are carried forward into the prediction. The benefits of a denser MD network are most evident during the cycling period and early forecast hours. With increasing forecast lead time, however, RMSEs continue to grow and the

https://doi.org/10.5194/egusphere-2026-3350
Preprint. Discussion started: 31 August 2026

differences among sensitivity experiments gradually diminish. Overall, assimilation of MD observations with higher horizontal resolution improves both temperature and moisture analyses and leads to corresponding gains in short-term forecasts.

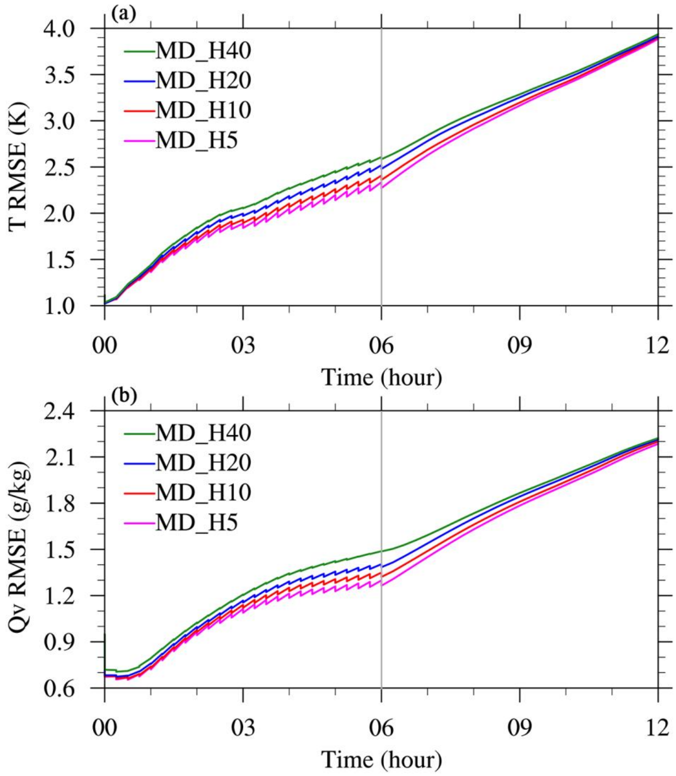

Figure 6. Impact of horizontal resolution on RMSEs of thermodynamic analyses and forecasts.

Time series of domain-averaged root-mean-square errors (RMSEs) for (a) temperature (K), and (b) specific humidity (g kg^{-1}) analyses and forecasts from the MD_H40 (green), MD_H20 (blue), MD_H10 (red), and MD_H5 (magenta) experiments. The thin grey line separates analysis cycling and 6-h free forecasts.

4.1.2 Impact on precipitation forecasts

The 3-, 6-, and 9-h accumulated precipitation forecasts from NoDA and the first set of DA experiments, are compared with the truth simulation in Fig. 7 and 8. All DA forecasts are initialized from the final analysis at the end of assimilation cycles. For

https://doi.org/10.5194/egusphere-2026-3350
Preprint. Discussion started: 31 August 2026

the truth simulation, the rainfall system evolves from a relatively compact southwest-northeast-oriented band at 3 h into a more organized mesoscale rainband extending across central Hebei and southern Beijing at 6 h, followed by a concentrated heavy rain center over the central and eastern parts of Beijing at 9 h (Fig. 7a-c). In contrast, the NoDA experiment exhibits substantial precipitation forecast errors, characterized by markedly weaker precipitation over Beijing and central Hebei province, and overpredicted rainfall in Shanxi province, resulting in a less coherent representation of the primary rainband, especially at 3- and 6-h forecast lead times (Fig. 7 d-f). In addition, NoDA fails to reproduce the narrow heavy-rain band over eastern Hebei near the coast seen in the truth simulation. Assimilation of MD observations overall improves the location, continuity, and orientation of the forecast rainband. Relative to NoDA, the DA experiments better reproduce the northeastward extension of the rainfall system and reduce the separation between the western and eastern precipitation cores, while also capturing the narrow coastal heavy-rain band over eastern Hebei province, albeit with slightly overpredicted intensity. The improvement becomes generally more evident as the observation density increases from 40 to 5 km (Fig. 7g-i, Fig. 8), indicating that denser MD networks provide more effective constraints on the mesoscale thermodynamic structure relevant to precipitation evolution. Among the DA experiments, MD_H10 and MD_H5 show the closest agreement with the truth, with a better-defined central rainband and reduced spatial displacement. In particular, MD_H5 gives the closest placement of the primary heavy-rain band, whereas coarser networks, especially MD_H40, tend to place the rainband too far north and overestimate the areal coverage of precipitation. Nevertheless, all experiments still retain some deficiencies in the location and intensity of the heavy precipitation forecasts, with the rainband displaced to the north to varying degrees in all DA experiments. This likely reflects the fact that the assimilated MD observations are limited to below 1 km and thus can only partially constrain the thermodynamic structure of a deep convective system, while the associated adjustment to the dynamical field through assimilation of thermodynamic

https://doi.org/10.5194/egusphere-2026-3350
Preprint. Discussion started: 31 August 2026

observations alone remains relatively weak.

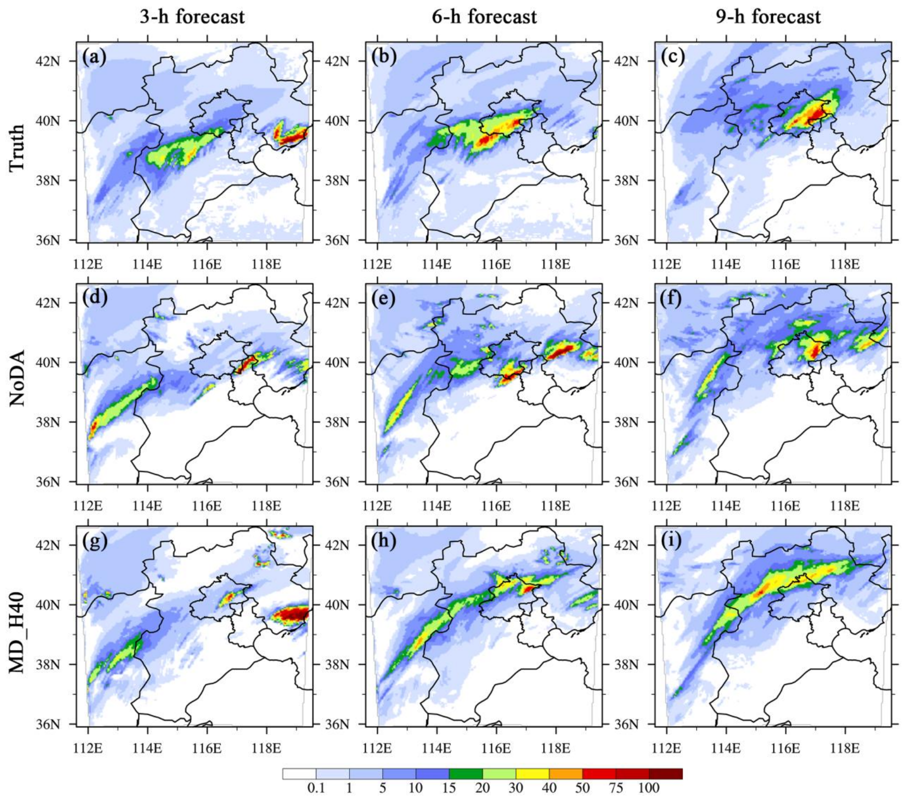

Figure 7. Impact of horizontal resolution on precipitation forecasts.

The 3-hourly accumulated precipitation forecasts (mm, shaded) for (a)-(c) Truth, (d)-(f) NoDA, and (g)-(i) MD_H40 experiments initiated at 1800 UTC 29 July 2024. The (left) 3-, (middle) 6-, and (right) 9-h forecasts are shown.

https://doi.org/10.5194/egusphere-2026-3350
Preprint. Discussion started: 31 August 2026

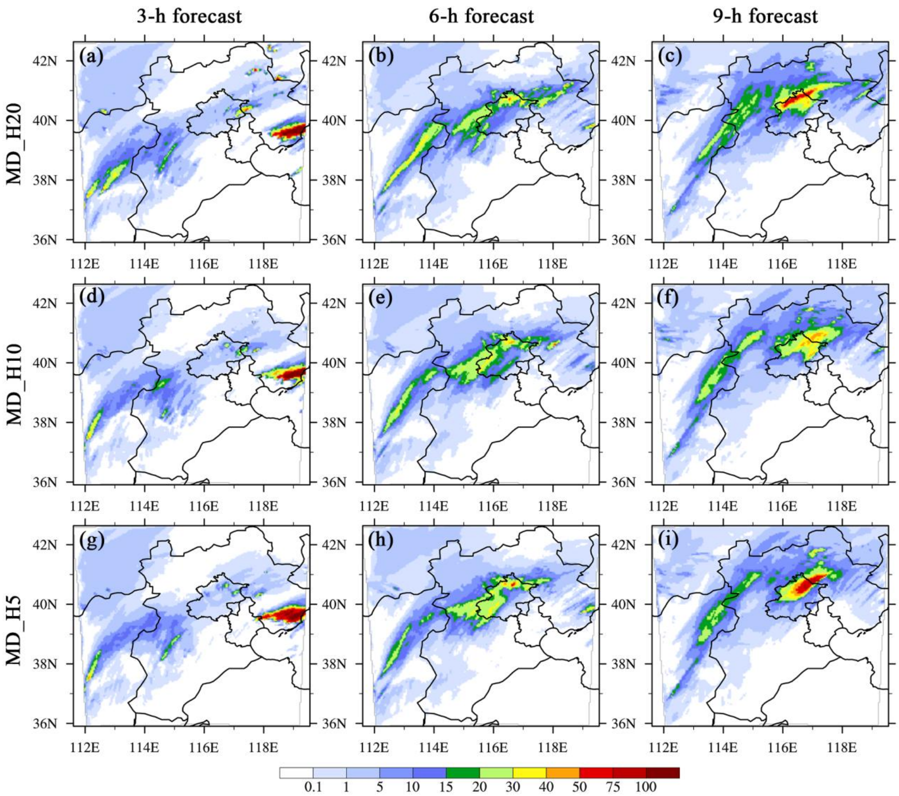

Figure 8. Continued from Fig. 7.

Same as in Fig. 7, but for the accumulated precipitation forecasts (mm, shaded) from (a)–(c) MD_H20, (d)–(f) MD_H10, and (g)–(i) MD_H5 experiments.

https://doi.org/10.5194/egusphere-2026-3350
Preprint. Discussion started: 31 August 2026

To quantify the performance of precipitation forecasts by assimilating MD data with different horizontal resolutions, neighborhood-based ETS and categorical performance diagrams are derived for the 1-9 h hourly precipitation amount (HPRCP) forecasts initialized at the end of the DA cycles (Fig. 9). All metrics are evaluated using a 12-km neighborhood radius. In the performance diagrams, higher forecast skill is associated with larger POD, SR, and CSI values and therefore points closer to the upper-right corner, while BIAS values larger (smaller) than 1.0 indicate overprediction (underprediction). Consistent with the spatial distribution of precipitation forecasts shown in Fig. 7 and 8, all DA experiments, except MD_H40, generally outperform NoDA throughout 1-9 h forecast period, indicating an overall positive impact of MD DA on short-term precipitation forecasts. However, MD_H40 shows slightly degraded forecast skill at some forecast lead times, which may be partly attributed to the fact that the 40-km MD network is too coarse to adequately represent mesoscale and smaller-scale thermodynamic structures, as evidenced by the residual temperature and moisture biases over Beijing and the upstream mountainous region (Fig. 4c and Fig. 5c). MD_H5 and MD_H10 remain closest to the upper-right portion of the performance diagrams and retain the largest ETS values for most forecast lead times, followed by MD_H20, while MD_H40 has the poorest forecast skills among all DA experiments. As the rainfall threshold increases from 5 to 15 mm, forecast skill decreases in all experiments, as reflected by lower POD, SR, CSI, and ETS values, but the relative ranking remains broadly similar. It is worth noting that the skill advantage of MD_H5 is most pronounced at the 15-mm threshold. Collectively, these score metrics support the visual impression from Fig. 7 and 8 that denser MD networks, especially those with 10- and 5-km grid spacing, more effectively predict the precipitation evolution and yield more accurate quantitative precipitation forecasts.

https://doi.org/10.5194/egusphere-2026-3350
Preprint. Discussion started: 31 August 2026

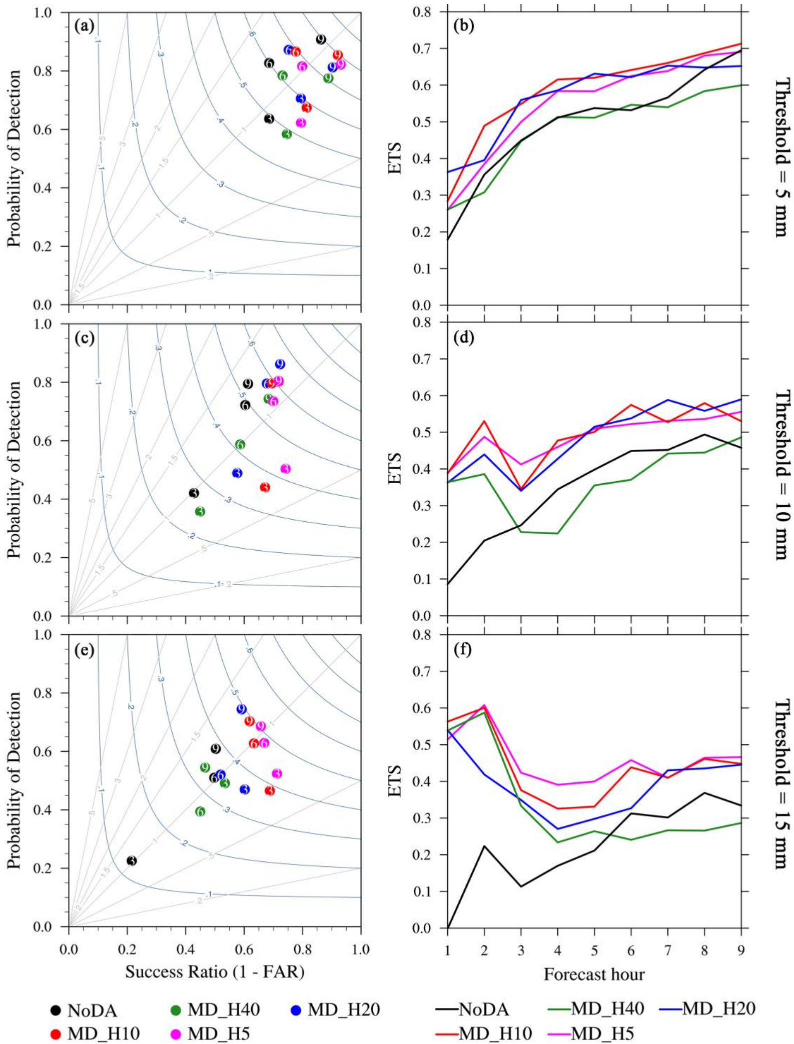

Figure 9. Impact of horizontal resolution on score metrics of precipitation forecast.

Score metrics of 1-9 h hourly precipitation amount (HPRCP) forecasts for the NoDA (black), MD_H40 (green), MD_H20 (blue), MD_H10 (red), and MD_H5 (magenta) experiments. (left) The performance diagrams, and (right) the equitable threat score (ETS) for (a)–(b) 5 mm, (c)–(d) 10 mm, and (e)–(f) 15 mm thresholds, respectively. Results are shown for a neighborhood radius of 12-km. The numbers within the colored dots in the performance diagrams denote the forecast hour (i.e., 3-, 6-, and 9-h forecasts).

https://doi.org/10.5194/egusphere-2026-3350
Preprint. Discussion started: 31 August 2026

Overall, the results in this section indicate that increasing the horizontal resolution of MD observations improves the representation of the lower-tropospheric thermodynamic structure, as reflected by reduced temperature and humidity analysis and forecast errors. The thermodynamic improvements contribute to more accurate precipitation forecasts, including better rainband placement, a more realistic representation of rainfall intensity, and higher quantitative precipitation forecast skill. Among the tested configurations, the 5- and 10-km MD observation networks show the most consistent benefits, suggesting that relatively dense MD observations are more effective for improving convective-scale short-term precipitation forecasts.

4.2 Sensitivity to observation height and spatial distribution

Given the generally positive impact of dense MD observations shown above, a natural next question is how the analysis and forecast sensitivity depends on the vertical placement and spatial deployment of the MD network. To address this issue, the experiments in this section compare three single-level MD assimilation configurations (i.e. the MD_H5_Z120, MD_H5_Z300, and MD_H5_Z600 experiments), in which observations are sampled at 120, 300, and 600 m, respectively, along with an additional experiment (MD_H5_Plain) in which the MD network is restricted to the plain area with terrain elevation below 300 m. These representative observation heights are chosen to reflect realistic low-altitude MD operations in China and are broadly consistent with typical operating levels within the PBL (Fig. 2). As the MD_H5 experiment shows the superior performance in Sect. 4.1, all sensitivity experiments in this section are performed using the 5-km MD network as the reference configuration.

Figure 10 compares the vertical profiles of domain-averaged RMSEs for temperature and specific humidity analyses from the second and third sets of DA experiment and the baseline experiment. As illustrated in Fig. 10a, the temperature RMSE profiles are broadly similar among the experiments in the middle and upper troposphere, and the primary differences are evident in the lower troposphere (below 700 hPa). The strongest sensitivity is found below about 800 hPa, where the analysis

https://doi.org/10.5194/egusphere-2026-3350
Preprint. Discussion started: 31 August 2026

is most directly constrained by the assimilated MD observations. Within this layer, the baseline experiment MD_H5 yields the smallest temperature RMSEs, whereas the single-level DA experiments show varying degrees of degradation, with the magnitude and vertical distribution of the errors depending on the observation height. This indicates that observations distributed over multiple levels provide better adjustments on the lower-tropospheric thermal structure than observations limited to a single height. Among the three single-level experiments, MD_H5_Z600 and MD_H5_Z300 generally outperform MD_H5_Z120 throughout most levels. It is also noticed that the level where each single-level RMSE profile most closely matches that of MD_H5 shifts upward with increasing observation height, consistent with the vertical placement of the assimilated observations. On the other hand, the near-surface temperature RMSE becomes larger as the observation height rises. By contrast, MD_H5_Plain exhibits the largest temperature RMSEs through most levels, except near the lowest level, where its analysis error is slightly smaller than that of MD_H5_Z600. This suggests that restricting the MD network to the plain area degrades the temperature analysis relative to the full-network configuration, likely because the largest temperature errors are mainly located over the mountainous region (Fig. 4b).

The humidity RMSE profiles exhibit a vertical dependence similar to that of temperature, with relatively small differences among the experiments in the middle and upper troposphere and stronger sensitivity in the lower troposphere (Fig. 10b). Compared with the temperature analysis, however, the inter-experiment spread is significantly larger below 700 hPa, indicating a stronger sensitivity of the moisture analysis to MD observation height and network deployment. MD_H5 again yields the smallest humidity RMSEs overall. And the single-level experiments show larger errors, with MD_H5_Z120 performing the worst and the level of closest agreement with MD_H5 shifting upward as the observation height increases. As in the temperature field, restricting the network to the plain area similarily degrades the humidity analysis, and MD_H5_Plain exhibits relatively larger RMSEs across much

https://doi.org/10.5194/egusphere-2026-3350
Preprint. Discussion started: 31 August 2026

of the lower troposphere. Overall, the moisture analysis is more sensitive than temperature to both observation height and spatial distribution of MD data, while the assimilation of multi-level MD observations provides the greatest improvement in the lower-tropospheric moisture structure.

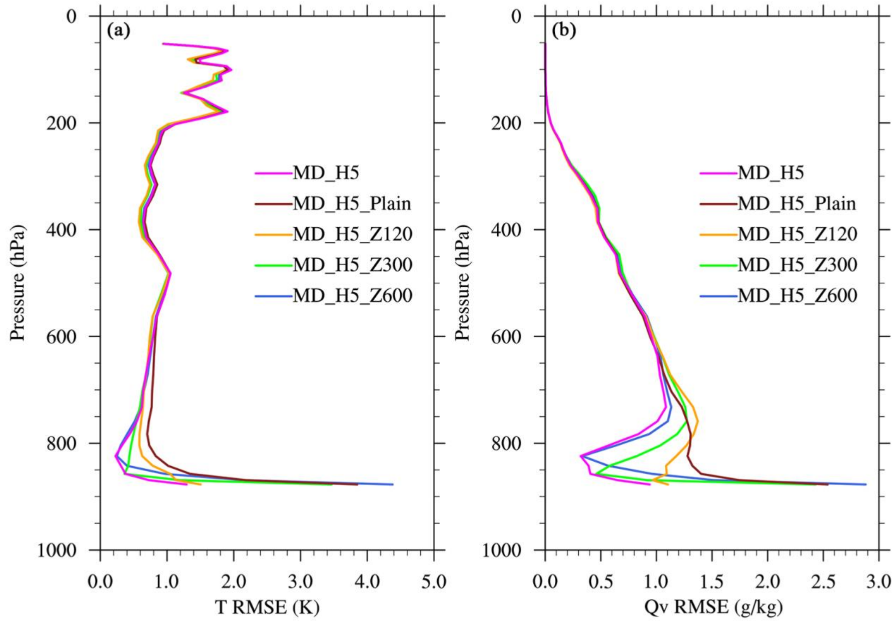

Figure 10. Impact of observation height and spatial distribution on RMSE profiles of temperature and humidity analyses.

Vertical profiles of domain-averaged RMSEs for (a) temperature (K), and (b) specific humidity (g kg^{-1}) analyses at 1800 UTC 29 July 2024 (end of the assimilation cycles) from the MD_H5 (magenta), MD_H5_Plain (brown), MD_H5_Z120 (orange), MD_H5_Z300 (green), and MD_H5_Z600 (blue) experiments.

https://doi.org/10.5194/egusphere-2026-3350
Preprint. Discussion started: 31 August 2026

To assess the impact of different observation heights and spatial distributions of MD data on precipitation forecasts, neighborhood-based ETS and performance diagrams for the sensitivity and baseline experiments are compared in Fig. 11. At the 5-mm threshold, all experiments show generally good forecast skill, but MD_H5_Z600 exhibits superior performance throughout most forecast lead times, with the highest ETS, CSI, POD, and SR values and a BIAS closest to 1, followed closely by the baseline experiment MD_H5 (Fig. 11a and b). Among the remaining sensitivity experiments, MD_H5_Z120 performs slightly better during the 1-3 h forecast period, whereas MD_H5_Z300 becomes more skillful at later forecast lead times. By contrast, the MD_H5_Plain experiment tends to show inferior performance throughout most of the forecast period at the threshold of 5 mm. As the threshold increases to 10 and 15 mm, the differences among the experiments become more pronounced. For the 10-mm threshold, MD_H5 and MD_H5_Z600 show comparable performance and remain the most skillful experiments (Fig. 11 c and d). Unlike the 5-mm threshold, MD_H5_Plain performs much better than MD_H5_Z300 and MD_H5_Z120 during the first 3 h, while these three experiments exhibit similar forecast skill thereafter. At the 15-mm threshold, the baseline experiment MD_H5 shows overwhelming superiority over the other DA experiments, followed by MD_H5_Z600, whereas the plain-only and lower-level configurations remain less skillful (Fig. 11 e and f). These results suggest that, within the tested height range, MD observations extending to higher levels are generally more beneficial for precipitation forecasts than those confined to the lowest level alone, while the multi-level MD DA still provides the most robust overall improvement. In addition, the degraded performance of the plain-only experiment highlights the importance of MD thermodynamic observations over the upstream mountainous regions, where the temperature and humidity errors are relatively large and where convection is initiated before moving downstream into the plains.

https://doi.org/10.5194/egusphere-2026-3350
Preprint. Discussion started: 31 August 2026

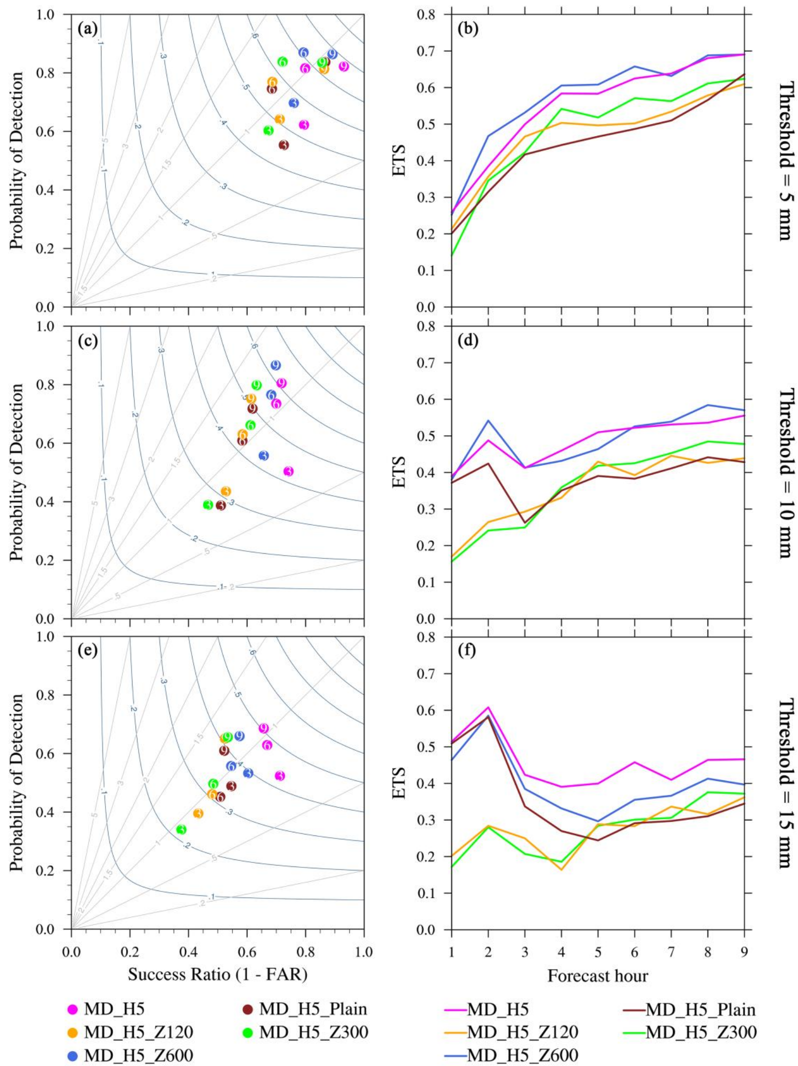

Figure 11. Impact of observation height and spatial distribution on precipitation forecasts.

Same as Fig. 9, but for the MD_H5 (magenta), MD_H5_Plain (brown), MD_H5_Z120 (orange), MD_H5_Z300 (green), and MD_H5_Z600 (blue) experiments.

https://doi.org/10.5194/egusphere-2026-3350
Preprint. Discussion started: 31 August 2026

4.3 Sensitivity to joint thermodynamic-wind assimilation and observation error

The results above indicate assimilation of synthetic MD thermodynamic observations can benefit convective-scale precipitation forecasts. Since the evolution of convection also depends strongly on the dynamical environment, it is further examined here whether the assimilation of MD wind observations together with temperature and humidity data provides additional forecast skill. A related issue is how sensitive is the assimilation performance to the assumed quality of the MD observations. To address these questions, the experiments in this section investigate the added value of jointly assimilating thermodynamic and wind observations, as well as the sensitivity of the analyses and forecasts to prescribed observation errors in temperature, humidity, and wind, respectively.

The influence of jointly assimilating MD wind observations with temperature and humidity can be straightforwardly assessed by examining the temperature, specific humidity, and wind departures from the truth (Fig. 12). The overall temperature error pattern at 850 hPa remains similar between MD_H5 and MD_H5_UV, with residual warm biases along the northern mountainous region and weak cold biases over offshore area (Fig. 12a and b). For the humidity analysis, the error patterns in MD_H5 and MD_H5_UV are also broadly similar (Fig. 12c and d), indicating that the additional assimilation of wind observations has only a limited effect on the thermodynamic analyses. In Contrast, the MD_H5_UV experiment substantially reduces the wind errors relative to MD_H5, particularly along the Taihang Mountains and the coastal area, where the lower-tropospheric flow structure is remarkably better captured. This suggests that assimilating MD wind data together with temperature and humidity observations not only improves the thermodynamic analyses, but also yields a more pronounced additional benefit in optimizing the lower-tropospheric dynamical field.

https://doi.org/10.5194/egusphere-2026-3350
Preprint. Discussion started: 31 August 2026

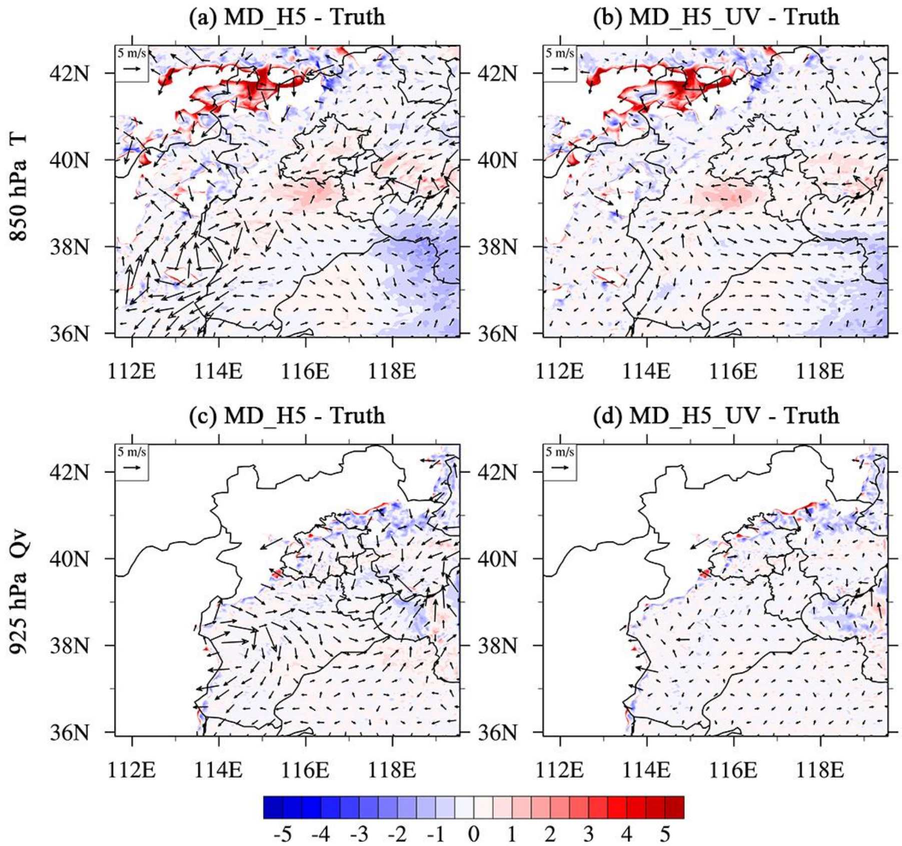

Figure 12. Impact of joint assimilation of thermodynamic and wind observations on analyses.

(a) Differences in 850-hPa temperature (°C, shaded) and wind (vectors) between the MD_H5 experiment and the truth run at 1800 UTC 29 July 2024 (end of the assimilation cycles). (b) As in (a), but for the MD_H5_UV experiment. (c) Differences in 925-hPa specific humidity (g kg^{-1}, shaded) and wind (vectors) between the MD_H5 experiment and the truth run. (d) As in (c), but for MD_H5_UV.

https://doi.org/10.5194/egusphere-2026-3350
Preprint. Discussion started: 31 August 2026

Figure 13 illustrates the sensitivity of the analyses to inflated observation errors for temperature, humidity, and wind observations, respectively. To highlight the differences among the sensitivity experiments, this figure shows the vertical profiles of RMSE differences relative to the MD_H5_UV experiment, such that positive values (to the right of the gray line in Fig. 13) represent degraded analyses under inflated observation errors. The response is clearly variable dependent, with the most pronounced degradations generally occurring in the lower troposphere, where the MD observations provide the strongest constraint. As expected, increasing the temperature (humidity) observation error mainly degrades the temperature (humidity) analysis, especially below about 700 hPa, while its impact on the humidity (temperature) analysis remains comparatively limited (Fig. 13a and b). Moreover, inflated temperature or humidity observation error also increases the wind RMSEs in both the upper and lower troposphere (Fig. 13c and d). This behavior suggests that, although the thermodynamic analyses are adjusted primarily by their respective observations, the resulting thermal perturbations can still affect the wind analysis through hydrostatic and mass-wind balance relationships embedded in the variational system. By contrast, increasing the wind observation error produces the largest degradations in both the u and v analyses, whereas its impact on the thermodynamic analyses remains relatively small, which agrees well with the earlier finding that the additional assimilation of wind observation exerts only a limited influence on the thermodynamic analyses (Fig. 12). Overall, the analysis is controlled primarily by the observation error standard deviations of the directly assimilated variables, while cross-variable correlations allow part of the observational information, and its associated error, to be distributed to related fields. These results emphasize that the quality of MD observations is critical for obtaining an accurate lower-tropospheric analysis, and that consistency between thermodynamic and wind observations is also important for maintaining a balanced and dynamically coherent analysis.

https://doi.org/10.5194/egusphere-2026-3350
Preprint. Discussion started: 31 August 2026

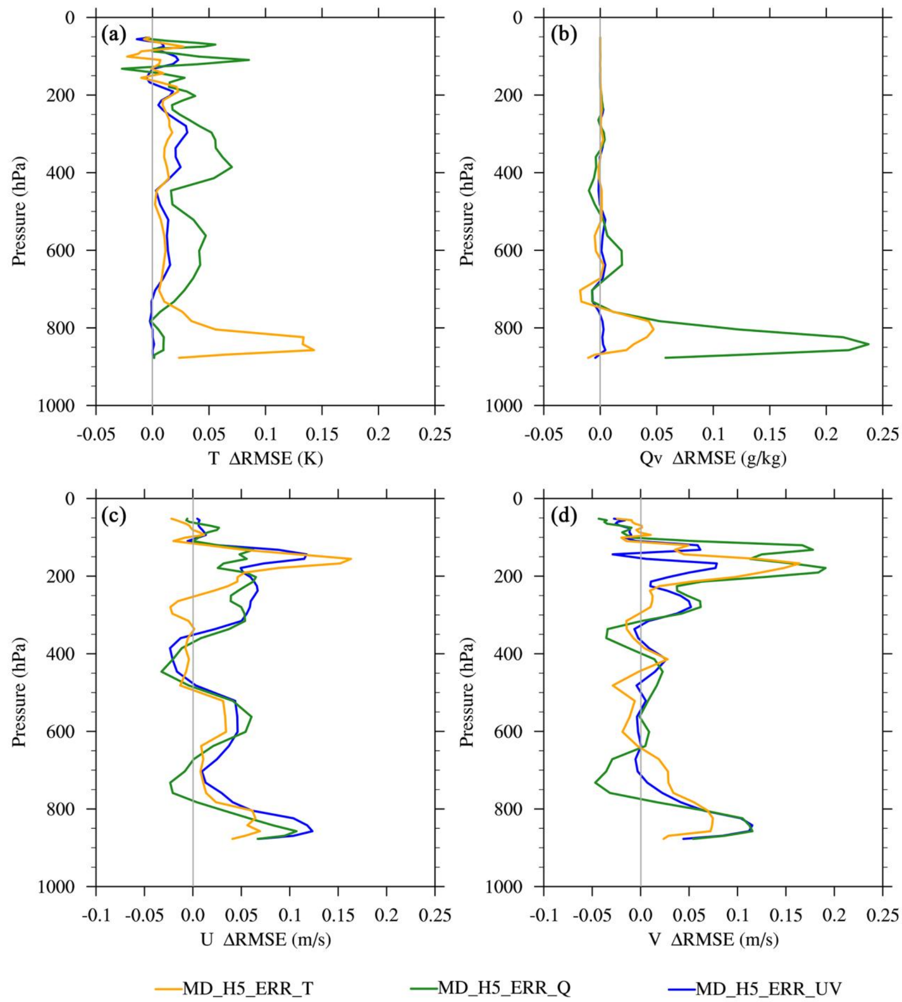

Figure 13. Impact of inflated observation errors on analysis RMSEs.

Vertical profiles of (a) temperature (K), (b) specific humidity (g kg^{-1}), (c) u (m s^{-1}), and (d) v (m s^{-1}) analysis RMSE differences for the MD_H5_ERR_T (orange), MD_H5_ERR_Q (green), and MD_H5_ERR_UV (blue) experiments relative to the MD_H5_UV experiment at 1800 UTC 29 July 2024. The gray vertical line denotes zero RMSE difference; positive values to the right of the line indicate degraded analysis.

To provide an overall assessment of the effects of joint thermodynamic-wind assimilation and observation error on precipitation forecasts, quantitative verification

https://doi.org/10.5194/egusphere-2026-3350
Preprint. Discussion started: 31 August 2026

metrics including ETS, BIAS, POD, and FAR for the 6-h accumulated precipitation forecast are compared among the MD_H5, MD_H5_UV, MD_H5_ERR_T, MD_H5_ERR_Q, and MD_H5_ERR_UV experiments (Fig. 14). Compared with the thermodynamic-only baseline experiment MD_H5, the joint assimilation experiment MD_H5_UV consistently yields higher ETS and POD values, and lower FARs at all thresholds, together with a modest increase in BIAS. This indicates that incorporating wind observations improves precipitation forecasts without substantially increasing overprediction. This is mainly attributed to improvements in the lower-tropospheric wind analyses by joint thermodynamic-wind assimilation (Fig. 12), underscoring the importance of PBL flow field in the convective-scale precipitation forecast. Additionally, the sensitivity to prescribed observation error is also evident in Fig. 14. At the lower thresholds of 2.5 and 5 mm, the differences among the DA experiments are relatively small, suggesting that light-to-moderate rainfall forecasts are less sensitive to the assumed MD observation quality (Fig. 14a and b). At the 10- and 15-mm thresholds, however, the contrasts become more pronounced (Fig. 14c and d). Although the ETS and POD (FAR) scores from the three inflated-error joint assimilation experiments are lower (higher) than those of MD_H5_UV, they still generally outperform MD_H5 across most thresholds. Regarding BIAS, a slight underprediction (overprediction) bias is observed for all DA experiments at the 2.5 and 5 mm (10 and 15 mm) thresholds. Among the three error-inflation experiments, MD_H5_ERR_UV shows the most evident reduction in forecast skill overall, indicating that rainfall prediction is especially sensitive to the wind observation errors. By contrast, MD_H5_ERR_Q exhibits a somewhat different behavior from MD_H5_ERR_T and MD_H5_ERR_UV, with ETS slightly higher than that of MD_H5_UV and FAR occasionally lower at some thresholds (e.g. 10 and 15 mm). Several factors may contribute to this result. First, the precipitation forecast in this case appears to be more sensitive to the retained wind and temperature constraints than to a moderate degradation of the humidity analysis. Second, inflating the humidity observation error may weaken the direct moisture adjustment and thus reduce localized moisture overcorrection, which can in turn suppress overpredicted precipitation in northern Beijing. Third, as the variational assimilation system distributes observational information through coupled thermodynamic and dynamical balance relationships, and the model forecast between assimilation cycles further enforces consistency among variables, part of the loss of humidity information may be compensated for by the remaining temperature and wind observations.

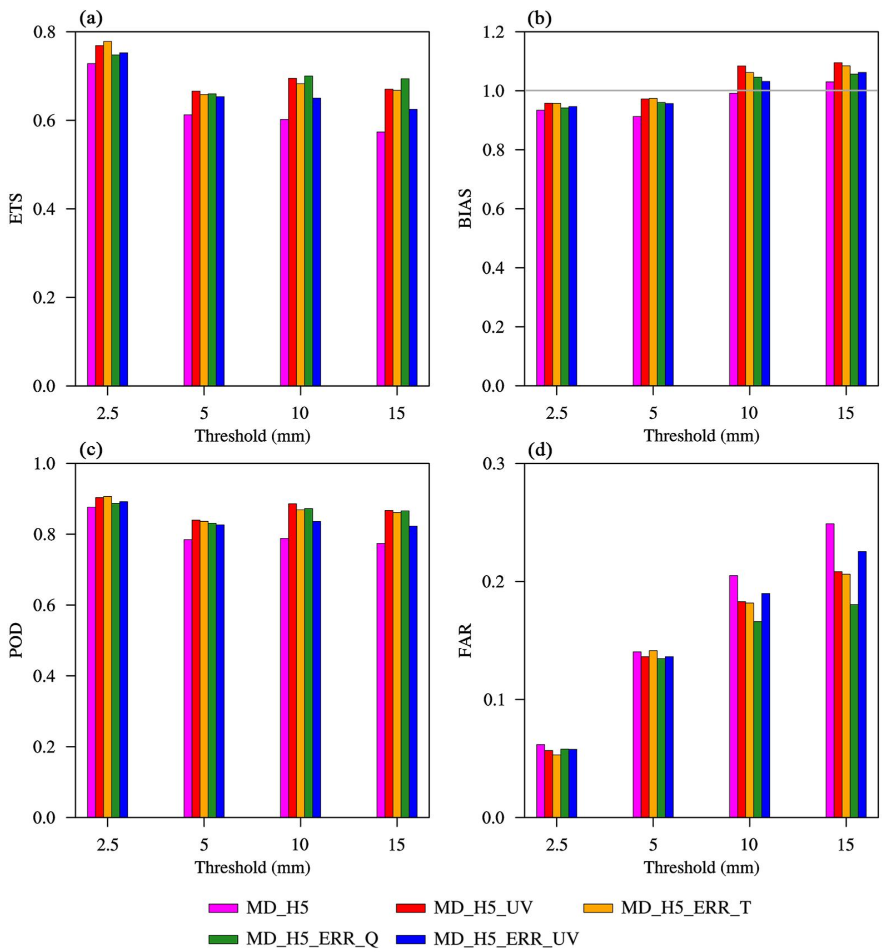

Figure 14. Impact of joint assimilation and observational error on precipitation forecasts.

(a) The equitable threat score (ETS) , (b) bias, (c) probability of detection (POD), and (d) false alarm ratio (FAR) of 6-hourly accumulated precipitation forecasts from the

https://doi.org/10.5194/egusphere-2026-3350
Preprint. Discussion started: 31 August 2026

MD_H5 (magenta), MD_H5_UV (red), MD_H5_ERR_T (orange), MD_H5_ERR_Q (green), and MD_H5_ERR_UV (blue) experiments at 2.5-, 5-, 10-, and 15-mm thresholds, respectively.

In summary, jointly assimilating wind observations with temperature and humidity provides clear additional benefits over the thermodynamic DA alone. Although the thermodynamic analysis fields are only slightly modified by wind DA, the lower-tropospheric flow is significantly improved, and this dynamical improvement leads to more skillful 6-h precipitation forecasts. The observation-error sensitivity experiments further show that the forecast benefit is also sensitive to the assumed quality of MD data, with the most pronounced degradation in forecast skill occurring when the wind observation error is inflated. These findings highlight the importance of both accurately representing the PBL airflow and maintaining high-quality, internally consistent thermodynamic and wind observations for improving convective-scale analyses and precipitation forecasts.

5. Summary and conclusions

This research investigates the potential impact of MD observations on convective-scale analyses and short-term precipitation forecasts through an OSSE framework. Synthetic MD observations of temperature, specific humidity, and horizontal winds are generated from the free-running truth simulation and assimilated into the convective-scale DA system NSSL3DVAR. A series of sensitivity experiments is conducted to examine how MD network horizontal resolution, observation height, spatial distribution, joint thermodynamic-wind assimilation, and observation errors affect the analyses and forecasts.

The results indicate that the horizontal resolution of the MD network has a pronounced impact on both thermodynamic analyses and precipitation forecasts. Assimilating higher-horizontal-resolution MD data yields smaller temperature and humidity errors during the assimilation cycles and subsequent short-term forecasts, as well as improved precipitation forecasts in terms of rainband placement, rainfall

https://doi.org/10.5194/egusphere-2026-3350
Preprint. Discussion started: 31 August 2026

intensity, and quantitative score metrics. Among the tested configurations, the 5- and 10-km networks provide the most consistent benefits, whereas the 40-km network is too coarse to adequately resolve the mesoscale and smaller-scale thermodynamic structures relevant to convective precipitation evolution.

Sensitivity experiments on observation height reveal that the impact of MD observations also depends on their vertical placement within the PBL. Multi-level MD DA provides the most balanced improvements in both temperature and humidity analyses, while single-level observations confined to the lower levels are less effective. In general, assimilation of observations extending to higher levels (i.e. 600 m) is more beneficial for precipitation forecasts than those limited to the lowest level alone. In addition, the inferior forecast performance in the plain-only DA experiment also underscores the value of MD observations over the upstream mountainous areas, where larger thermodynamic errors persist and where the convection system in this case is initiated and intensifies before propagating into the downstream plains.

The joint assimilation of MD wind observations with thermodynamic data further improves the analyses and forecasts. The additional assimilation of wind observations substantially reduces wind analysis errors, especially over the Taihang Mountains and the coastal areas, although it produces only very small additional adjustments to the temperature and humidity analyses beyond those already achieved by thermodynamic observations. This dynamical improvement leads to more skillful precipitation forecasts, indicating that an accurate representation of the PBL flow is important for convective-scale precipitation prediction. The observation-error sensitivity experiments further demonstrate that forecast skill is also influenced by the assumed quality of MD observations, with inflated wind observation error producing the most pronounced degradation in precipitation forecast performance. These results indicate that the impact of MD observations depends not only on the availability of both thermodynamic and wind measurements, but also on their resolution, vertical distribution, and accuracy and mutual dynamical and thermodynamic consistency.

Overall, the OSSE results consistently demonstrate that MD observations have considerable potential to improve convective-scale analyses and short-term precipitation forecasts. The greatest forecast benefits are achieved when the MD network is sufficiently dense, spans multiple levels within the PBL, incorporates wind observations, and samples the upstream mountainous region where convection is initiated. Meanwhile, the results also suggest that the forecast impact remains sensitive to the observation error standard deviations and to the limited vertical extent of low-altitude MD measurements. The insights gained from this OSSE study can help guide the optimal design of MD observation networks over the BTH region.

Although this study shows encouraging results of assimilating simulated MD data into a convective-scale model, several limitations should be noted. First, only synthetic MD observations are assimilated, while conventional observations (e. g., radiosonde and surface data) as well as radar and satellite observations are excluded. This experimental design facilitates a clearer attribution of forecast impacts to MD observations, while the forecast improvements reported here should therefore be interpreted as an estimate of the maximum potential impact of MD observations. In operational applications, where conventional observations are already assimilated, the incremental benefit of MD observations may be smaller and warrants further investigation. Second, the MD observations are confined to the lower troposphere (below 1 km), consistent with current low-altitude MD deployment strategies in China, so their ability to constrain the full-depth thermodynamic structure of deep convection remains limited. Third, the conclusions are based on a heavy rainfall event occurred over the Beijing-Tianjin-Hebei region. Additional cases covering different synoptic and convective environments and regions are needed to assess the robustness and generality of these findings. Future work should therefore extend the present framework to multiple cases, incorporate MD observations together with other dense observations, and further evaluate optimal strategies for network density, observation height, and adaptive deployment. Moreover, the benefits of assimilating real MD observations for convective-scale NWP can be investigated once operational MD networks become available. Such efforts will provide a more comprehenive assessment of the practical value of MD observations for convective-scale NWP and short-term high-impact weather forecasting.

Code and data availability

The ERA5 reanalysis and GFS forecast data are accessible from ECMWF (https://www.ecmwf.int/en/forecasts/datasets/reanalysis-datasets/era5/, Hersbach et al., 2020) and National Centers for Environmental Prediction, National Weather Service, NOAA, US Department of Commerce (https://doi.org/10.5065/D65D8PWK, National Centers for Environmental Prediction et al., 2015), respectively. The source code for WRF model version 3.7.1 and the input ERA5 and GFS data used in this study have been archived on Zenodo at https://doi.org/10.5281/zenodo.19691512 (Zhao, 2026a). The namelist files for WRF and the assimilation system used in this study are accessible online (https://doi.org/10.5281/zenodo.19691638, Zhao, 2026b).

Author contributions

JZ and JPG conceptualized this study. JZ executed the experiments, analyzed the results, and wrote the original draft. JPG supervised the project, delivered key suggestions during experiments, and participated in manuscript revision. JDG provided guidance for the DA method and contributed to the revision of the manuscript. HLY provided guidance on the design of the MD observation networks.

Competing interests

The contact author has declared that none of the authors has any competing interests.

Acknowledgements

This work was jointly supported by the National Natural Science Foundation of China under grants 42325501, 42530610, 42375018, and 42561160141, the China Meteorological Administration Training Centre Key Research Program under grant

https://doi.org/10.5194/egusphere-2026-3350
Preprint. Discussion started: 31 August 2026

2026CMATCZDIAN09, the Anhui Provincial Science and Technology Tackling Plan under grant 202523t06050001, and Innovation and Development Special Project of the China Meteorological Administration under grant CXFZ2026J107. This work comprised regular duties at federally funded NOAA/NSSL for J. Gao. ChatGPT (GPT-5.5; OpenAI's large-scale language-generation model) was used to improve the writing style of this article.

References

Bell, T. M., Greene, B. R., Klein, P. M., Carney, M., and Chilson, P. B.: Confronting the boundary layer data gap: evaluating new and existing methodologies of probing the lower atmosphere, Atmos. Meas. Tech., 13, 3855–3872, https://doi.org/10.5194/amt-13-3855-2020, 2020.

Benjamin, S. G., Grell, G. A., Brown, J. M., Smirnova, T. G., and Bleck, R.: Mesoscale Weather Prediction with the RUC Hybrid Isentropic–Terrain-Following Coordinate Model, Monthly Weather Review, 132, 473–494, https://doi.org/10.1175/1520-0493(2004)132%3C0473:MWPWTR%3E2.0.CO;2, 2004.

Chilson, P. B., Bell, T. M., Brewster, K. A., Britto Hupsel De Azevedo, G., Carr, F. H., Carson, K., Doyle, W., Fiebrich, C. A., Greene, B. R., Grimsley, J. L., Kanneganti, S. T., Martin, J., Moore, A., Palmer, R. D., Pillar-Little, E. A., Salazar-Cerreno, J. L., Segales, A. R., Weber, M. E., Yeary, M., and Droegemeier, K. K.: Moving towards a Network of Autonomous UAS Atmospheric Profiling Stations for Observations in the Earth's Lower Atmosphere: The 3D Mesonet Concept, Sensors, 19, 2720, https://doi.org/10.3390/s19122720, 2019.

Clark, A. J., Gallus, W. A., and Weisman, M. L.: Neighborhood-Based Verification of Precipitation Forecasts from Convection-Allowing NCAR WRF Model Simulations and the Operational NAM, Weather and Forecasting, 25, 1495–1509, https://doi.org/10.1175/2010WAF2222404.1, 2010.

Crook, N. A.: Sensitivity of Moist Convection Forced by Boundary Layer Processes to Low-Level Thermodynamic Fields, Mon. Wea. Rev., 124, 1767–1785, https://doi.org/10.1175/1520-0493(1996)124%3C1767:SOMCFB%3E2.0.CO;2, 1996.

De Boer, G., Butterworth, B. J., Elston, J. S., Houston, A., Pillar-Little, E., Argrow, B., Bell, T. M., Chilson, P., Choate, C., Greene, B. R., Islam, A., Martz, R., Rhodes, M., Rico, D., Stachura, M., Lappin, F. M., Segales, A. R., Whyte, S., and Wilson, M.: Evaluation and Intercomparison of Small Uncrewed Aircraft Systems Used for Atmospheric Research, Journal of Atmospheric and Oceanic Technology, 41, 127–145, https://doi.org/10.1175/JTECH-D-23-0067.1, 2024.

Dudhia, J.: Numerical Study of Convection Observed during the Winter Monsoon Experiment Using a Mesoscale Two-Dimensional Model, Journal of Atmospheric Sciences, 46, 3077–3107, https://doi.org/10.1175/1520-0469(1989)046%3C3077:NSOCOD%3E2.0.CO;2, 1989.

Fierro, A. O., Wang, Y., Gao, J., and Mansell, E. R.: Variational Assimilation of Radar Data and GLM Lightning-Derived Water Vapor for the Short-Term Forecasts of High-Impact Convective Events, Monthly Weather Review, 147, 4045–4069, https://doi.org/10.1175/MWR-D-18-0421.1, 2019.

Gao, J. and Stensrud, D. J.: Assimilation of Reflectivity Data in a Convective-Scale, Cycled 3DVAR Framework with Hydrometeor Classification, Journal of the Atmospheric Sciences, 69, 1054–1065, https://doi.org/10.1175/JAS-D-11-0162.1, 2012.

Gao, J. and Stensrud, D. J.: Some Observing System Simulation Experiments with a Hybrid 3DEnVAR System for Storm-Scale Radar Data Assimilation, Monthly Weather Review, 142, 3326–3346, https://doi.org/10.1175/MWR-D-14-00025.1, 2014.

Gao, J., Xue, M., Brewster, K., and Droegemeier, K. K.: A Three-Dimensional Variational Data Analysis Method with Recursive Filter for Doppler Radars, Journal of Atmospheric and

Oceanic Technology, 21, 457–469, https://doi.org/10.1175/1520-0426(2004)021%3C0457:ATVDAM%3E2.0.CO;2, 2004.

Gao, J., Smith, T. M., Stensrud, D. J., Fu, C., Calhoun, K., Manross, K. L., Brogden, J., Lakshmanan, V., Wang, Y., Thomas, K. W., Brewster, K., and Xue, M.: A Real-Time Weather-Adaptive 3DVAR Analysis System for Severe Weather Detections and Warnings, Weather and Forecasting, 28, 727–745, https://doi.org/10.1175/WAF-D-12-00093.1, 2013.

Gao, J., Fu, C., Stensrud, D. J., and Kain, J. S.: OSSEs for an Ensemble 3DVAR Data Assimilation System with Radar Observations of Convective Storms, Journal of the Atmospheric Sciences, 73, 2403–2426, https://doi.org/10.1175/JAS-D-15-0311.1, 2016.

Gao, J., Heinselman, P. L., Xue, M., Wicker, L. J., Yussouf, N., Stensrud, D. J., and Droegemeier, K. K.: The Numerical Prediction of Severe Convective Storms: Advances in Research and Applications, Remaining Challenges, and Outlook for the Future, in: Encyclopedia of Atmospheric Sciences, edited by Robinson, W. A., Vol. 1, Elsevier/Academic Press, 372 – 393, https://doi.org/10.1016/B978-0-323-96026-7.00127-2, 2024.

Ge, G., Gao, J., and Xue, M.: Diagnostic Pressure Equation as a Weak Constraint in a Storm-Scale Three-Dimensional Variational Radar Data Assimilation System, Journal of Atmospheric and Oceanic Technology, 29, 1075–1092, https://doi.org/10.1175/JTECH-D-11-00201.1, 2012.

Heinselman, P. L., Burke, P. C., Wicker, L. J., Clark, A. J., Kain, J. S., Gao, J., Yussouf, N., Jones, T. A., Skinner, P. S., Potvin, C. K., Wilson, K. A., Gallo, B. T., Flora, M. L., Martin, J., Creager, G., Knopfmeier, K. H., Wang, Y., Matilla, B. C., Dowell, D. C., Mansell, E. R., Roberts, B., Hoogewind, K. A., Stratman, D. R., Guerra, J., Reinhart, A. E., Kerr, C. A., and Miller, W.: Warn-on-Forecast System: From Vision to Reality, Weather and Forecasting, 39, 75–95, https://doi.org/10.1175/WAF-D-23-0147.1, 2024.

Hersbach, H., Bell, B., Berrisford, P., Hirahara, S., Horányi, A., Muñoz-Sabater, J., Nicolas, J., Peubey, C., Radu, R., Schepers, D., Simmons, A., Soci, C., Abdalla, S., Abellan, X., Balsamo, G., Bechtold, P., Biavati, G., Bidlot, J., Bonavita, M., De Chiara, G., Dahlgren, P., Dee, D., Diamantakis, M., Dragani, R., Flemming, J., Forbes, R., Fuentes, M., Geer, A., Haimberger, L., Healy, S., Hogan, R. J., Hólm, E., Janisková, M., Keeley, S., Laloyaux, P., Lopez, P., Lupu, C., Radnoti, G., De Rosnay, P., Rozum, I., Vamborg, F., Villaume, S., and Thépaut, J.: The ERA5 global reanalysis, Quart J Royal Meteoro Soc, 146, 1999–2049, https://doi.org/10.1002/qj.3803, 2020.

Hoffman, R. N. and Atlas, R.: Future Observing System Simulation Experiments, Bulletin of the American Meteorological Society, 97, 1601–1616, https://doi.org/10.1175/BAMS-D-15-00200.1, 2016.

Hoffmann, L., Günther, G., Li, D., Stein, O., Wu, X., Griessbach, S., Heng, Y., Konopka, P., Müller, R., Vogel, B., and Wright, J. S.: From ERA-Interim to ERA5: the considerable impact of ECMWF's next-generation reanalysis on Lagrangian transport simulations, Atmos. Chem. Phys., 19, 3097–3124, https://doi.org/10.5194/acp-19-3097-2019, 2019.

Hong, S.-Y., Noh, Y., and Dudhia, J.: A New Vertical Diffusion Package with an Explicit Treatment of Entrainment Processes, Monthly Weather Review, 134, 2318–2341, https://doi.org/10.1175/MWR3199.1, 2006.

Houston, A. L., Walther, J. C., Pytlikzillig, L. M., and Kawamoto, J.: Initial Assessment of Unmanned Aircraft System Characteristics Required to Fill Data Gaps for Short-term Forecasts: Results from Focus Groups and Interviews, J. Operational Meteor., 111–120,

https://doi.org/10.5194/egusphere-2026-3350
Preprint. Discussion started: 31 August 2026

https://doi.org/10.15191/nwajom.2020.0809, 2020.

Hu, H., Sun, J., and Zhang, Q.: Assessing the Impact of Surface and Wind Profiler Data on Fog Forecasting Using WRF 3DVAR: An OSSE Study on a Dense Fog Event over North China, Journal of Applied Meteorology and Climatology, 56, 1059–1081, https://doi.org/10.1175/JAMC-D-16-0246.1, 2017.

Hu, J., Yussouf, N., Turner, D. D., Jones, T. A., and Wang, X.: Impact of Ground-Based Remote Sensing Boundary Layer Observations on Short-Term Probabilistic Forecasts of a Tornadic Supercell Event, Weather and Forecasting, 34, https://doi.org/10.1175/waf-d-18-0200.1, 2019.

Hu, J., Fierro, A. O., Wang, Y., Gao, J., and Mansell, E. R.: Exploring the Assimilation of GLM-Derived Water Vapor Mass in a Cycled 3DVAR Framework for the Short-Term Forecasts of High-Impact Convective Events, Monthly Weather Review, 148, 1005–1028, https://doi.org/10.1175/MWR-D-19-0198.1, 2020.

Hu, J., Gao, J., Wang, Y., Pan, S., Fierro, A. O., Skinner, P. S., Knopfmeier, K., Mansell, E. R., and Heinselman, P. L.: Evaluation of an experimental WARN-ON-FORECAST 3DVAR analysis and forecast system on quasi-real-time short-term forecasts of high-impact weather events, Quart J Royal Meteoro Soc, 147, 4063–4082, https://doi.org/10.1002/qj.4168, 2021.

Huang, Y., Wang, X., Mahre, A., Yu, T.-Y., and Bodine, D.: Impacts of assimilating future clear-air radial velocity observations from phased array radar on convection initiation forecasts: An observing system simulation experiment study, Monthly Weather Review, https://doi.org/10.1175/MWR-D-21-0199.1, 2022.

Huo, Z., Liu, Y., Shi, Y., Chen, B., Fan, H., and Li, Y.: An Investigation on Joint Data Assimilation of a Radar Network and Ground-Based Profiling Platforms for Forecasting Convective Storms, Monthly Weather Review, 151, 2049–2064, https://doi.org/10.1175/MWR-D-22-0332.1, 2023.

Inoue, J., Seko, H., Sato, K., and Sakai, T.: Operational Capability of Drone-Based Meteorological Profiling in an Urban Area, JGR Atmospheres, 130, e2024JD041927, https://doi.org/10.1029/2024JD041927, 2025.

Jensen, A. A., Pinto, J. O., Bailey, S. C. C., Sobash, R. A., De Boer, G., Houston, A. L., Chilson, P. B., Bell, T., Romine, G., Smith, S. W., Lawrence, D. A., Dixon, C., Lundquist, J. K., Jacob, J. D., Elston, J., Waugh, S., and Steiner, M.: Assimilation of a Coordinated Fleet of Uncrewed Aircraft System Observations in Complex Terrain: EnKF System Design and Preliminary Assessment, Monthly Weather Review, 149, 1459–1480, https://doi.org/10.1175/MWR-D-20-0359.1, 2021.

Jiang, Y., Xin, J., Wang, Y., Tang, G., Zhao, Y., Jia, D., Zhao, D., Wang, M., Dai, L., Wang, L., Wen, T., and Wu, F.: The thermodynamic structures of the planetary boundary layer dominated by synoptic circulations and the regular effect on air pollution in Beijing, Atmos. Chem. Phys., 21, 6111–6128, https://doi.org/10.5194/acp-21-6111-2021, 2021.

Jones, T. A., Wang, X., Skinner, P., Johnson, A., and Wang, Y.: Assimilation of GOES-13 Imager Clear-Sky Water Vapor (6.5 μm) Radiances into a Warn-on-Forecast System, Monthly Weather Review, 146, 1077–1107, https://doi.org/10.1175/MWR-D-17-0280.1, 2018.

Kay, J., Pinto, J. O., Weckwerth, T. M., and De Boer, G.: Quantifying UAS Observation Error Variance Used in Data Assimilation Systems and Its Impact on Predictive Skill, J Adv Model Earth Syst, 17, e2024MS004601, https://doi.org/10.1029/2024MS004601, 2025.

https://doi.org/10.5194/egusphere-2026-3350
Preprint. Discussion started: 31 August 2026

Leuenberger, D., Haefele, A., Omanovic, N., Fengler, M., Martucci, G., Calpini, B., Fuhrer, O., and Rossa, A.: Improving High-Impact Numerical Weather Prediction with Lidar and Drone Observations, Bulletin of the American Meteorological Society, 101, E1036–E1051, https://doi.org/10.1175/BAMS-D-19-0119.1, 2020.

Li, N., Guo, J., Wu, M., Zhang, F., Guo, X., Sun, Y., Zhang, Z., Liang, H., and Chen, T.: Low-Level Jet and Its Effect on the Onset of Summertime Nocturnal Rainfall in Beijing, Geophysical Research Letters, 51, e2024GL110840, https://doi.org/https://doi.org/10.1029/2024GL110840, 2024.

Mallick, S. and Jones, T. A.: Assimilation of GOES-16 satellite derived winds into the warn-on-forecast system, Atmospheric Research, 245, 105131, https://doi.org/10.1016/j.atmosres.2020.105131, 2020.

Mansell, E. R. and Ziegler, C. L.: Aerosol Effects on Simulated Storm Electrification and Precipitation in a Two-Moment Bulk Microphysics Model, Journal of the Atmospheric Sciences, 70, 2032–2050, https://doi.org/10.1175/JAS-D-12-0264.1, 2013.

Mansell, E. R., Ziegler, C. L., and Bruning, E. C.: Simulated Electrification of a Small Thunderstorm with Two-Moment Bulk Microphysics, Journal of the Atmospheric Sciences, 67, 171–194, https://doi.org/10.1175/2009JAS2965.1, 2010.

Mlawer, E. J., Taubman, S. J., Brown, P. D., Iacono, M. J., and Clough, S. A.: Radiative transfer for inhomogeneous atmospheres: RRTM, a validated correlated-k model for the longwave, J. Geophys. Res., 102, 16663–16682, https://doi.org/10.1029/97JD00237, 1997.

Murdzek, S. S., Ladwig, T. T., Houston, A. L., and James, E. P.: The Impacts of Assimilating Various Densities of Uncrewed Aircraft System Observations on Regional NWP Forecasts in an OSSE, Monthly Weather Review, 154, 955–976, https://doi.org/10.1175/MWR-D-25-0175.1, 2026.

National Centers for Environmental Prediction, National Weather Service, NOAA, U.S. Department of Commerce: NCEP GFS 0.25 Degree Global Forecast Grids Historical Archive, https://doi.org/https://doi.org/10.5065/D65D8PWK, 2015.

Pan, S., Gao, J., Stensrud, D. J., Wang, X., and Jones, T. A.: Assimilation of Radar Radial Velocity and Reflectivity, Satellite Cloud Water Path, and Total Precipitable Water for Convective-Scale NWP in OSSEs, Journal of Atmospheric and Oceanic Technology, 35, 67–89, https://doi.org/10.1175/JTECH-D-17-0081.1, 2018.

Pan, S., Gao, J., Jones, T. A., Wang, Y., Wang, X., and Li, J.: The Impact of Assimilating Satellite-Derived Layered Precipitable Water, Cloud Water Path, and Radar Data on Short-Range Thunderstorm Forecasts, Monthly Weather Review, 149, 1359–1380, https://doi.org/10.1175/MWR-D-20-0040.1, 2021.

Pang, Z., Shi, C., Gu, J., Pan, Y., and Xu, B.: Assessment of a Gauge-Radar-Satellite Merged Hourly Precipitation Product for Accurately Monitoring the Characteristics of the Super-Strong Meiyu Precipitation over the Yangtze River Basin in 2020, Remote Sensing, 13, 3850, https://doi.org/10.3390/rs13193850, 2021.

Pinto, J. O., O'Sullivan, D., Taylor, S., Elston, J., Baker, C. B., Hotz, D., Marshall, C., Jacob, J., Barfuss, K., Piguet, B., Roberts, G., Omanovic, N., Fengler, M., Jensen, A. A., Steiner, M., and Houston, A. L.: The Status and Future of Small Uncrewed Aircraft Systems (UAS) in Operational Meteorology, Bulletin of the American Meteorological Society, 102, E2121–E2136, https://doi.org/10.1175/BAMS-D-20-0138.1, 2021.

https://doi.org/10.5194/egusphere-2026-3350
Preprint. Discussion started: 31 August 2026

Pinto, J. O., Bailey, S. C. C., Fossell, K. R., Binau, S., Xu, M., Kay, J., Nolin, R. D., Vezzi, C. N., Smith, S. W., Lave, J., Colavito, J., Wilson, M. B., and Weckwerth, T. M.: Impact of Assimilating Uncrewed Aircraft System Observations on River Valley Fog Prediction, Weather and Forecasting, 39, 1673–1694, https://doi.org/10.1175/WAF-D-23-0087.1, 2024.

Purser, R. J., Wu, W.-S., Parrish, D. F., and Roberts, N. M.: Numerical Aspects of the Application of Recursive Filters to Variational Statistical Analysis. Part I: Spatially Homogeneous and Isotropic Gaussian Covariances, Monthly Weather Review, 131, 1524–1535, https://doi.org/10.1175//1520-0493(2003)131%3C1524:NAOTAO%3E2.0.CO;2, 2003a.

Purser, R. J., Wu, W. S., Parrish, D. F., and Roberts, N. M.: Numerical Aspects of the Application of Recursive Filters to Variational Statistical Analysis. Part II: Spatially Inhomogeneous and Anisotropic General Covariances, Monthly Weather Review, 131, 1536–1548, 2003b.

Reuder, J., Jonassen, M. O., and Ólafsson, H.: The Small Unmanned Meteorological Observer SUMO: Recent developments and applications of a micro-UAS for atmospheric boundary layer research, Acta Geophys., 60, 1454–1473, https://doi.org/10.2478/s11600-012-0042-8, 2012.

Segales, A. R., Greene, B. R., Bell, T. M., Doyle, W., Martin, J. J., Pillar-Little, E. A., and Chilson, P. B.: The CopterSonde: an insight into the development of a smart unmanned aircraft system for atmospheric boundary layer research, Atmos. Meas. Tech., 13, 2833–2848, https://doi.org/10.5194/amt-13-2833-2020, 2020.

Skamarock, W., Klemp, J., Dudhia, J., Gill, D., Barker, D., Wang, W., Huang, X.-Y., and Duda, M.: A Description of the Advanced Research WRF Version 3, UCAR/NCAR, https://doi.org/10.5065/D68S4MVH, 2008.

Sun, Q., Vihma, T., Jonassen, M. O., and Zhang, Z.: Impact of Assimilation of Radiosonde and UAV Observations from the Southern Ocean in the Polar WRF Model, Adv. Atmos. Sci., 37, 441–454, https://doi.org/10.1007/s00376-020-9213-8, 2020.

Wang, Y., Gao, J., Skinner, P. S., Knopfmeier, K., Jones, T., Creager, G., Heiselman, P. L., and Wicker, L. J.: Test of a Weather-Adaptive Dual-Resolution Hybrid Warn-on-Forecast Analysis and Forecast System for Several Severe Weather Events, Weather and Forecasting, 34, 1807–1827, https://doi.org/10.1175/WAF-D-19-0071.1, 2019.

Weckwerth, T. M. and Parsons, D. B.: A Review of Convection Initiation and Motivation for IHOP_2002, Monthly Weather Review, 134, 5–22, https://doi.org/10.1175/MWR3067.1, 2006.

Wen, Q., Zhang, X., Hu, S., Zhao, P., Zhong, S., Liu, Z., Zhao, Z., Liang, J., Dai, G., Zhang, C., Li, M., and Huang, L.: Collaborative assimilation experiment of Beidou radiosonde and drone-dropped radiosonde based on CMA-TRAMS, Atmospheric and Oceanic Science Letters, 18, 100555, https://doi.org/10.1016/j.aosl.2024.100555, 2025.

Zhang, L. and Pu, Z.: An Observing System Simulation Experiment (OSSE) to Assess the Impact of Doppler Wind Lidar (DWL) Measurements on the Numerical Simulation of a Tropical Cyclone, Advances in Meteorology, 2010, 743863, https://doi.org/10.1155/2010/743863, 2010.

Zhang, W., Guo, J., Miao, Y., Liu, H., Song, Y., Fang, Z., He, J., Lou, M., Yan, Y., Li, Y., and Zhai, P.: On the Summertime Planetary Boundary Layer with Different Thermodynamic Stability in China: A Radiosonde Perspective, Journal of Climate, 31, 1451–1465, https://doi.org/10.1175/JCLI-D-17-0231.1, 2018.

https://doi.org/10.5194/egusphere-2026-3350
Preprint. Discussion started: 31 August 2026

Zhao, J.: WRF model and the input ERA5 reanalysis and GFS forecast data [Data set]. Zenodo. https://doi.org/10.5281/zenodo.19691512, 2026a.

Zhao, J.: Namelist files for WRF and the assimialtion system [Data set]. Zenodo. https://doi.org/10.5281/zenodo.19691638, 2026b.

Zhao, J., Gao, J., Jones, T. A., and Hu, J.: Impact of Assimilating High-Resolution Atmospheric Motion Vectors on Convective Scale Short-Term Forecasts: 1. Observing System Simulation Experiment (OSSE), Journal of Advances in Modeling Earth Systems, 13, e2021MS002484, https://doi.org/https://doi.org/10.1029/2021MS002484, 2021a.

Zhao, J., Gao, J., Jones, T. A., and Hu, J.: Impact of Assimilating High-Resolution Atmospheric Motion Vectors on Convective Scale Short-Term Forecasts: 2. Assimilation Experiments of GOES-16 Satellite Derived Winds, J Adv Model Earth Syst, 13, e2021MS002486, https://doi.org/10.1029/2021MS002486, 2021b.

Zhao, J., Gao, J., Jones, T., and Hu, J.: Impact of Assimilating High-Resolution Atmospheric Motion Vectors on Convective Scale Short-Term Forecasts: 3. Experiments With Radar Reflectivity and Radial Velocity, Journal of Advances in Modeling Earth Systems, 14, e2022MS003246, https://doi.org/https://doi.org/10.1029/2022MS003246, 2022.

Zhao, J., Guo, J., and Zheng, X.: Impact of multiple radar wind profiler data assimilation on convective-scale short-term rainfall forecasts: OSSE studies over the Beijing–Tianjin–Hebei region, Geosci. Model Dev., 18, 4075–4101, https://doi.org/10.5194/gmd-18-4075-2025, 2025.

Zhuang, Z., Yussouf, N., and Gao, J.: Analyses and forecasts of a tornadic supercell outbreak using a 3DVAR system ensemble, Advances in Atmospheric Sciences, 33, 544–558, https://doi.org/10.1007/s00376-015-5072-0, 2016.

Ziegler, C. L.: Retrieval of Thermal and Microphysical Variables in Observed Convective Storms. Part 1: Model Development and Preliminary Testing, Journal of Atmospheric Sciences, 42, 1487–1509, https://doi.org/10.1175/1520-0469(1985)042%3C1487:ROTAMV%3E2.0.CO;2, 1985.